1-31-2013

Topological dynamics of spike-timing dependent plastic neural networks

David Stone

David B. Stone
Candidate

Psychology
Department

This dissertation is approved, and it is acceptable in quality and form for publication:

Approved by the Dissertation Committee:

Claudia D. Tesche, Chairperson

Thomas P. Caudell

Vincent P. Clark

Derek A. Hamilton

TOPOLOGICAL DYNAMICS OF SPIKE-TIMING DEPENDENT PLASTIC NEURAL NETWORKS

By

David B. Stone

B.S., Psychology, The University of New Mexico, 2000
M.S., Psychology, The University of New Mexico, 2009

DISSERTATION

Submitted in Partial Fulfillment of the
Requirements for the Degree of

Doctor of Philosophy
Psychology

The University of New Mexico
Albuquerque, New Mexico

December 2012

Dedication

I dedicate this work to Claudia, who gave me a chance when no one else would.

TOPOLOGICAL DYNAMICS OF SPIKE-TIMING DEPENDENT PLASTIC NEURAL NETWORKS

By

DAVID B. STONE

B.S., Psychology, The University of New Mexico, 2000
M.S., Psychology, The University of New Mexico, 2009
Ph.D., Psychology, The University of New Mexico, 2012

ABSTRACT

The effects of continual spike-timing dependent plasticity (STDP) on the topology of evolving neural networks were assessed. After a period of stabilization, a number of topological features were monitored periodically throughout simulations of network activity to quantify changes in network structure. Under a range of different input regimes and initial network configurations, each network maintained a robust and highly stable global structure. At the same time, a substantial set of small three-neuron subgraphs (triads) continued to undergo an array of changes and revealed a dynamic local topology. These findings suggest that on-going STDP provides an efficient means of selecting and maintaining a stable yet flexible network organization.

Table of Contents

List of Figures

List of Tables

Chapter 1

Introduction

Determining how populations of interacting neurons self-organize in the presence of noisy, rapidly changing stimuli and variable temporal and physical constraints remains a major challenge in neuroscience. In addition to the complex unfolding of developmental programs and environmentally driven modifications which occur early in life, neural networks continue to evolve throughout the lifespan. This on-going process of self-organization among interacting neurons is the central concern of this report.

One form of self-organization that has been extensively explored is spike-timing dependent plasticity, or STDP. As the name implies, STDP is a form of synaptic plasticity where changes in synaptic strength are determined by the timing of pre-synaptic and post-synaptic spikes: When the pre-synaptic neuron fires before the post-synaptic neuron, the synapse is potentiated, and when the post-synaptic neuron fires prior to the pre-synaptic neuron, the synapse is depressed. Since it was first characterized (Markram et al., 1997), STDP has been observed in a wide-range of neural systems, from mammalian cortical and sub-cortical networks to invertebrate nervous systems.

A number of models have been employed to explain some of the basic properties and consequences of STDP (e.g. Song et al., 2000). One approach that has been fruitful in characterizing the potential functionality of STDP has been to explore how it influences the structure (topology) of self-organizing neural networks. Graph theoretic measures borrowed from network science have revealed a number of adaptive topological features which emerge from STDP governed networks. For example, Shin and Kim (2006) demonstrated that a model network of excitatory and inhibitory neurons which employed STDP synaptic

modification developed small-world properties and power-law degree distributions. Small-world characteristics (i.e. high clustering and short average path lengths; Watts and Strogatz, 1998) have been detected in macaque and cat cortical networks, and the human reticular formation, and neuroimaging has revealed both small-world properties and power-law degree distributions in human functional brain networks (for a review of graph theoretical analyses of brain networks, see Reijneveld et al., 2007; Bullmore and Sporns, 2009). More recently, Ren et al. (2010) compared the local topological characteristics of the earthworm, *C. elegans* to a biologically inspired model STDP network. They found that the residual network evolved by STDP produced specific three-neuron connectivity patterns (motifs) in significantly greater frequencies than observed in comparable random networks. The profile of significant motifs types detected in their model network was qualitatively similar to those observed in the earthworm connectome. These studies suggest that STDP may be an underlying mechanism in evolving the neuronal topologies observed in some neurobiological systems.

While these and other studies have been informative regarding the role of STDP in developing adaptive topologies, they have failed to address the continual, experience dependent changes in network architecture which are likely influenced by on-going STDP. Several recent reports suggest that, in addition to its role in guiding cortical and subcortical structure during development, STDP continues to modify synaptic connectivity in mature neural networks. Yu et al. (2009) demonstrated that neurons in the superior colliculus of adult cats adapted their responses to cross-modal sensory stimuli over short time scales in a manner that was consistent with STDP governed synaptic modification. The authors suggest that, although not conclusive, STDP may remain a viable mechanism for rapid structural

modification well into adulthood. These results support a previous report of spike-timing dependent synaptic depression elicited in the primary somatosensory cortex of anesthetized adult rats by pairing whisker deflections with spontaneously emitted postsynaptic spikes or spikes generated by current injection (Jacob et al., 2007).

To date, there are only a few of studies that address the on-going topological dynamics of neural and brain systems. Robinson et al., (2009) tested the robustness and stability of different model network topologies during dynamic restructuring; however, their restructuring scheme was arbitrary, and analysis focused on properties of the emergent rather than the evolving architecture. In another study, Grindrod and Higham (2010) used a functional brain network to demonstrate the effectiveness of new algorithms in characterizing evolving graphs. Although interesting, the network used as an example was derived from a short sample of time-series EEG data and the algorithm was used to assess transient functional connectivity over a brief period of time.

The goal of this study was to explore the evolving topology of networks of neurons as they were modified by a biologically meaningful mechanism, on-going STDP. The outcome of this investigation revealed unique dynamic features of neural network topology that have not been observed in networks with static architectures and yielded new insights into the organizing principles of STDP that can only be captured during active network restructuring in the presence of continuous external input.

Chapter 2

Methods

Model Neural Networks

The model neural networks used in all simulations consisted of 400 regular-spiking excitatory (RSE) neurons and 100 fast-spiking inhibitory (FSI) interneurons. The neurons of each network were initially connected at random. The in-degrees and out-degrees (i.e. the number of pre- and post-synaptic connections) of each neuron were selected such that there were approximately 50 pre-synaptic and 50 post-synaptic synapses for each neuron (means = 50, s.d.'s = 5, normally distributed). Thus, there were approximately 25,000 synapses in each initial network (~10 % of full connectivity).

Izhikevich-type neurons were used in all network simulations (Izhikevich, 2004). The neuronal dynamics of both neuron types (RSE and FSI) were modeled by a system of differential equations:

Eq. 1 $$\frac{dV}{dt} = 0.04V^2 + 5V + 140 - u + I$$

Eq. 2 $$\frac{du}{dt} = a(bV - u),$$

where V is the neuronal membrane voltage (in millivolts, mV), u is a membrane relaxation variable, and I is the total input to the neuron (in mV). An action potential (spike) occurred when $V \geq 30$ mV, after which the voltage and relaxation variables were reset according to the equation:

Eq. 3 $$V \geq 30 : \{V \leftarrow c; u \leftarrow (u + d)\}$$

Eq. 1, 2, and 3, together with a range of values for parameters ***a***, ***b***, ***c***, and ***d***, allow a great variety of neuronal types and dynamics to be modeled. Based on previous work which explored different values (Izhikevich, 2004), the parameters for the RSE neurons were set to: ***a*** = 0.02, ***b*** = 0.2, ***c*** = -65 mV, and ***d*** = 8. For FSI neurons, the parameters were set to: ***a*** = 0.1, ***b*** = 0.2, ***c*** = -65 mV and ***d*** = 2. Note that parameters affecting the relaxation variable, ***u***, are modified for FSI neurons to shorten post-firing recovery which gives these neurons their fast-spiking behavior. The values of ***u*** and ***V*** were approximated using a fourth-order Runge-Kutta numerical method to evaluate *Eq.* 1, 2, and 3 (h = 0.5 timesteps for *Eq.* 1, and one timestep for *Eq.* 2 and 3). The simulation timestep was selected to approximate one millisecond (msec) of real time.

The excitatory post-synaptic weights were initially uniformly distributed between 0 and 8 mV (RSE→RSE synapses and RSE→FSI synapses), while initial inhibitory post-synaptic weights were distributed between -8 and 0 mV (FSI→RSE synapses and FSI→FSI synapses).

Network Input

Each network received five different types of external input in separate simulations. External stimulation varied in degree of regularity (periodicity) and synchrony and was qualitatively similar to the unique types of spiking network dynamics outlined by Brunel (2000). Under the regular, synchronous input regime (RS), a randomly selected subset of all neurons (mean = 100 neurons, s.d. = 1, normally distributed) received 16 mV input simultaneously every 20 timesteps (20 msec intervals, 50 Hz input rate). The subset of neurons receiving input changed on every input cycle (i.e. every 20 timesteps). The input parameters of the regular but asynchronous regime (RA) were the same as RS input except

that the input timing to each neuron was jittered around a mean of 20 msec with a 6 msec standard deviation. The third input regime simulated irregular (i.e. non-periodic), synchronous input (IS). Similar to RS input, a randomly selected subset of approximately 100 neurons received simultaneous input; however, input was delivered at a Poissonian distributed rate with a mean of 50 Hz. In the final two input regimes, input was delivered irregularly and asynchronously such that every neuron in the network received 16 mV input independently at a Poissonian distributed mean rate of either 50 Hz or 12 Hz (IA50 and IA12).

In addition to external input, every neuron in the network received a constant small subthreshold input at each timestep throughout the simulations. The value of this noisy input was picked each at each timestep from a Gaussian distribution with mean of 1.3 mV and standard deviation of 0.5 mV.

In addition to external input and subthreshold input, neurons in the network received input from their presynaptic neurons whenever the presynaptic neuron fired with a one msec delay. The magnitude of synaptic input was simply the weight of the synapse from the pre-synaptic neuron. The value of $\boldsymbol{I}$ in *Eq.* 1 is the linear sum of these three input terms for each neuron at every timestep.

Spike-Timing Dependent Plasticity

The weights of the RSE→RSE synapses in the network were modified for the duration of the simulation according to an asymmetric STDP learning rule. The STDP rule was implemented such that, when a pre-synaptic neuron fired before the post-synaptic neuron, the synapse connecting them was potentiated according to the equation:

Eq. 4 $$\Delta\omega_t = \Delta\omega_{t-1} + A_+ e^{-(tpost - tpre)/\tau},$$

and when the post-synaptic neuron fired before the pre-synaptic neuron, the synapse was depressed according to the equation:

Eq. 5 $$\Delta\omega_t = \Delta\omega_{t-1} + A_- e^{-(tpost - tpre)/\tau}$$

In *Eq.* 4 and 5, $\Delta\omega_t$ is the additive (+/-) change in synaptic weight, ***tpost*** and ***tpre*** are the post-synaptic and pre-synaptic firing times, respectively, $\Delta\omega_{t-1}$ is the value of $\Delta\omega$ from the preceding timestep, and τ is a time constant set to 20 msec which determines the width of the time window. The values of A_+ and A_- determine the maximum or minimum weight change for a given synaptic event (learning rate). The value of A_+ was set to 0.044 which is 0.55% of the maximal weight attainable by any synapse (8 mV). The value of A_- was set to -0.0462 to produce an asymmetry (bias toward synaptic depression) in the STDP rule. The values of τ, A_+, and A_- were selected based on the empirically derived STDP model outlined in Song et al., 2000.

The STDP rule was applied at all excitatory-to-excitatory synapses (RSE→RSE). $\Delta\omega$ was initially set to zero and *Eq.* 4 and 5 were evaluated during each timestep (each msec) of the simulation; however, the synapse was updated only once every 1000 timesteps (once per second) by adding the current value of $\Delta\omega$ at that timepoint to the current weight. Synaptic weights were bounded so that when the sum of the synaptic weight and $\Delta\omega$ was > 8 mV or < 0 mV, the weight was set to 8 mV or 0 mV, respectively.

To simulate on-going STDP and permit re-potentiation of zero-weight synapses, synapses with 0 mV weights were not removed from the network. Instead, the value of $\Delta\omega$

continued to be modified by *Eq.* 4 and 5 at each timestep and was added to the weight after every 1000 timesteps. Thus, re-potentiation could occur if **Δω** possessed a positive value when it was added to the current weight.

Simulations and Analysis

The dynamic effects of STDP on network topology were examined in ten separate model networks. Each network received each of the five external input regimes (RS, RA, IS, IA50, and IA12) in separate simulations resulting in 50 simulations total. Each simulation consisted of 7.2 million timesteps, or two hours of activity. Measures of global and local topological features were sampled once every 60,000 timesteps (every minute) during the last half of each simulation (The analysis interval; timesteps 3,600,001 to 7,200,000).

Global measures included the total number of excitatory-to-excitatory synapses in the network, the average weight of these synapses, and the average synaptic degree (the total pre-synaptic and post-synaptic excitatory-to-excitatory connections) per neuron at each sampling point.

In order to assess the stability of each of these measures across time, the coefficient of variation was also calculated for each measure, where the coefficient equals the standard deviation of the measure across the analysis interval divided by its mean. A smaller coefficient indicates more stability (i.e. less variation) across time. The coefficient of variation is a dimensionless quantity that permits direct comparisons of temporal stability between networks/simulations in circumstances where comparisons of means would be uninformative.

The potential small-world characteristics of the networks were also evaluated at by calculating the average clustering coefficients and path lengths across all excitatory neurons

at each sampling point in the analysis interval. The clustering coefficient is a measure that reflects the likelihood that two connected neurons (neighbors) would share a common neighbor. The clustering coefficient was determined in a manner which took into account both the strengths and directions of the synapses involved in each cluster and was based on a method presented in Fagiolo (2007). The clustering coefficient of each neuron was evaluated by the equation

Eq. 6

$$C_i = \frac{2}{k_i\left(k_i - 1\right) - 2\overleftrightarrow{k}_i} \sum_{j,m} \left(w_{ij} w_{im} w_{jm}\right)^{1/3},$$

where C_i is the clustering coefficient of neuron i and k_i is the total number of in-degrees and out-degrees of that neuron. $\overleftrightarrow{k}_i$ is the sum of bi-directional synapses of neuron i and its neighbors (i.e. where neuron i is both a pre-synaptic and post-synaptic neuron with its neighbor). w_{ij}, w_{im}, and w_{jm} are the synaptic weights between neuron i and its neighbor j, neuron i and its neighbor m, and the weight between the two neighbors, respectively. Note that *Eq.* 6 only takes into account those clusters that are purely directional (that contain no reciprocal synapses) and scales these clusters by the geometric mean of their synapses.

Path lengths were also determined in a manner that accounted for directionality and synaptic strength by employing Dijkstra's Algorithm (Dijkstra, 1959). This algorithm assumes that shortest distance between neuron i and neuron j is the directed distance between them containing the fewest synapses of the lowest magnitude. In the networks considered here, greater synaptic strengths should decrease distance (i.e. shorten paths).Since Dijkstra's Algorithm 'punishes' synapses of greater magnitude and rewards synapses of lower magnitude, the inverses of synaptic weights were used to assess path length.

Clustering coefficients and path lengths were averaged across all neurons at each sampling timepoint. The averages from each simulation were compared to the values from the initial randomly connected network. Higher clustering values and shorter path lengths than in the initial networks indicated an improved small-world topology. Both measures were calculated using functions included in the Brain Connectivity Toolbox (Rubinov and Sporns, 2010).

In order to quantify the local topological dynamics of each network, all three-neuron connected subgraphs (triads) present in each network at initialization were identified and changes in their synaptic connectivites were monitored during the analysis interval. There are 13 possible unique connectivity patterns in three-neuron subgraphs (Fig 1). The distributions of these 13 triad types in each network and their synaptic weights were assessed. Since only RSE $\rightarrow$ RSE synapses were subjected to the STDP learning rule, only triads comprised exclusively of excitatory neurons were considered in the analysis. Although on-going STDP permits the depression and repotentiation of existing synaptic connections, new synapses cannot be formed. Therefore, all of the triads identified in each of the ten initial networks may undergo state changes, but new triads cannot appear.

To determine the strength and stability of each triad, the synaptic intensities and coherences of the triad were measured during the analysis interval according to a method outlined by Onnela et al., 2005. The synaptic intensity of a triad is equivalent to the geometric mean of its synapses:

Eq. 7

$$I(s) = \left(\prod_{(i,j) \in N_s} w_{ij} \right)^{1/N_s},$$

where ***I(s)*** is the intensity of triad ***s***, N_s represents the number of synapses in ***s***, and w_{ij} refers to the synaptic strength of neuron ***i*** onto neuron ***j***. In the present scheme, intensities could range from 0 mV (non-connected) to 8 mV (the maximum allowable synaptic weight attainable). In addition, triad coherence is defined as the intensity of the triad (geometric mean) divided by its arithmetic mean:

Eq. 8

$$H(s) = \frac{I(s)}{\sum_{(i,j)\in N_s} w_{ij}},$$

where ***H(s)*** is the coherence of triad ***s***. The coherence of a triad is bounded between 0 and 1, and values approaching 1 occur when the synapses of the triad have nearly equal weights. Thus, coherence is a measure of triad synaptic stability.

Additional measures were calculated to evaluate the dynamics of individual triads across time. Potentially, a triad can 'disappear' when one or more of the synapses connecting the triad are lost and can re-emerge if the synapse(s) regain non-zero weights. Triads can also change triad type due to the loss or regain of their synapses (e.g. a type 5 triad could become a type 1, 2, or 3 triad due to the loss of one of its synapses). The total duration that a triad existed as one or more type during the interval was assessed. The value of triad duration was calculated as the percentage of sampling points in the analysis interval in which the triad appeared. The total number of state changes, including disappearances, re-emergences and type changes, was also assessed for each triad. An additional measure included each triad's repertoire size, i.e. the total number of triad types that the triad assumed during the analysis interval. As a final measure of triad dynamics, the total number of triads that re-emerged at a sampling point (triads gained), the total number that disappeared at that sampling point

(triads lost), and the net change in the total number of triads from one sampling point to the next were calculated.

For each of the measures mentioned, the effects of external input were assessed by performing a univariate analysis-of-variance (ANOVA) test on the measure where external input type was the fixed factor. When this test yielded a significance value of $p \leq 0$, separate t-tests were performed which contrasted the effects of synchronous vs asynchronous input (RS and IS vs RA, IA50, and IA 12) and regular vs irregular input (RS and RA vs IS, IA50, and IA 12) on the measure. These tests were Bonferroni corrected.

Motif analysis

Different types of small connected subgraphs present in complex networks are frequently referred to as "motifs". The original definition of network motifs provided by Milo et al., (2002) defined motifs as those subgraph types that occur in a network of interest at significantly greater frequencies than observed in equivalent, randomly connected networks of the same size. The significance of occurrences of each of the 13 possible different triad types was tested in the final organizations of the networks investigated (i.e. at the final timestep of each simulation). Final networks were compared to randomly connected networks where the random networks were generated by switching synapses between neurons in the final network while preserving the same number of incoming, outgoing, and mutual synapses of each neuron (mfinder, version 1.2, http://www.weizmann.ac.il/mcb/UriAlon). Between 50,000 and 100,000 switches were performed for each graph and 100 random graphs were generated for comparison. Details of the edge switching algorithm can be found in Milo et al., 2003.

For each of the 13 triad types, the number of occurrences of the type in the final network was compared to the number of occurrences of the type in 100 random networks by calculating a Z-score test statistic as follows:

Eq. 9

$$Z = \frac{F_{final} - F_{random}}{\sigma_{random}},$$

where F_{final} is the number of occurrences of the type in the final network and F_{random} and σ_{random} are the mean and standard deviation of the occurrences in the 100 random networks. If the Z-score was greater than 1.96 or less than -1.96, the type was considered to have occurred at significantly greater or fewer numbers than in the distribution of random networks (at the 95% confidence level) and therefore represented a significant motif in the final network.

Variations of STDP and Network Parameters

Several parameters of the STDP learning rule (*Eq.* 4 and 5) were modified to assess the effects upon network stability and dynamics. In the first modification, the values of A_+ and A_- were reduced to one tenth of their original values (0.0044 and - 0.0046, respectively; reduced STDP rate condition). In the second modification, the STDP time constant, τ, was reduced from 20 msec to 10 msec (reduced STDP window condition). In the final modification the asymmetry of the learning rule was removed such that $A_+ = A_- = 0.044$ (symmetric STDP condition). One simulation of each condition was conducted using each of the five external input regimes, resulting in 15 separate simulations. The same initial network was used for each simulation and was selected from the initial networks employed in the

original simulations. During the STDP modified simulations, all other parameters remained the same as in the original simulations.

Several measures were used to assess the effects of the STDP parameter modifications. The stabilities of global measures across time were evaluated by calculating the coefficient of variation of the number of RSE → RSE synapses remaining, the coefficient of variation of the average synaptic weight of these synapses, and the coefficient of variation of the average neuronal degree. Characteristics of triad dynamics were also evaluated for each modification, such as the percentage of triads remaining during the analysis interval, their dynamics, and their intensities and coherences. Changes in the number of triads and triad types across the analysis interval were also charted.

To assess the magnitude of the effects of these variations upon global and local network stability, direct comparisons were made between the original and parameter modified simulations by performing significance tests. These tests compared the coefficients of variation of synaptic number, synaptic weight, and neuronal degree from the original and modified simulations. The ratios of triad gains to net changes in triad counts (gained-to-net ratios) were also compared. T-scores were used as the test statistic and calculated as follows:

Eq. 10

$$t = \frac{V_{modified} - \overline{V}_{original}}{\sigma_{original} / \sqrt{n}},$$

$V_{modified}$ is the value of the measure resulting from the modified simulation and $\overline{V}_{original}$ and $\sigma_{original}$ are the mean and standard deviation of the value from the original simulations, respectively, and n is the sample size (10 in all cases examined). T-scores greater than 3.25 or

less than -3.25 were considered to be indications of a significant deviation in the measure from values obtained in the original simulations (at the 99% confidence interval). Comparisons were only made between simulations employing the same type of external input (e.g. STDP modified networks receiving RS type stimulation were only compared to the ten original simulations where RS stimulation was used).

In addition to modifications in the STDP learning rule, several modifications were also made to the configuration of the initial networks. In the first condition, the permissible range of synaptic weights was reduced from -8 to 8 mV to -4 to 4 mV while all other parameters remained the same (reduced synaptic weight condition). In the second condition, an asymmetry was introduced in the excitatory-to-inhibitory synaptic weight ratio such that the range of excitatory synaptic weights remained from 0 to 8 mV while the inhibitory range was increased from 0 to -8 mV to 0 to -9.6 mV (the asymmetric weight condition). In the third condition, the number of initial synapses was decreased from 25,000 to 12,500 (from 10% of full connectivity to 5% of full connectivity; the sparse connectivity condition). In the final modification, a subset of 100 neurons was randomly selected prior to the simulations, and only these neurons received external input (the stationary input condition). This condition contrasted with the original simulations where the subset of neurons receiving input changed during every input event. Each of these four modified networks received each of the five types of external input resulting in 20 additional simulations.

The global and local stabilities and dynamics of these configuration modified simulations were assessed using the same measures as above and the same test statistic (*Eq.* 10).

As a final test of the effects of on-going STDP on network topology, a simulation involving a different learning rule was implemented while network topology was assessed. This Hebbian-like learning rule was based on firing rate correlations between pre-synaptic and post-synaptic neurons and therefore served to contrast the timing dependence of STDP. Details of the implementation and results are presented in Appendix A.

Chapter 3

Results

Input Dependent Steady-State Network Activity Emerges During On-Going STDP

A pattern of steady-state synchronous firing activity emerged shortly after the beginning of each simulation. During this state, fluctuations in the average neuronal firing rates across time were marginal. Average neural firing rates for excitatory neurons are reported in Table I. Rates were determined by external stimulus type ($F(1,4) = 703.33$, $p < 0.001$) where irregular input patterns (IS, IA50, IA12) significantly increased firings of excitatory neurons ($t(48) = 3.52$, $p = 0.001$). Firing rates for RSE neurons from all simulations remained between 12 and 15 Hz. FSI neurons fired at almost twice that rate (overall mean = 29.68 Hz) owing to parameter differences in *Eq.* 2 and 3. Fig 2 shows exemplar network activity for each of the external input regimes.

A Stable Global Network Structure Emerges From On-Going STDP

Global topological features including the total number of synapses and their average synaptic weight, and average neuronal degree (number of synapses) were collected throughout the simulations and evaluated across the analysis interval. Table I and Fig 3 present the values of these global measures for each type of external input.

Each network initially possessed approximately 16,000 excitatory synapses of which an average of 9253.9 (s.d. = 207.30) or 57.8% (across all simulations) remained during analysis (i.e. these synapses possessed a strength greater than zero at least once during the analysis interval). For each simulation, the total number of synapses participating in the network remained highly stable across the interval (average coefficient of variation across all

simulations = 0.002, s.d. < 0.001). External input type had no significant effect on the number of remaining synapses or their stability across time ($p > 0.9$).

The overall average weight of excitatory synapses across all simulations was 4.48 mV (s.d. = 0.071), and the average coefficient of variation of these weights was 0.001 (s.d. < 0.001), revealing highly stable average synaptic strengths across time. A significant effect of input type on the average synaptic weight was detected ($F(1,4) = 222.42$, $p < 0.001$). Contrasts of the different input types revealed that synchronous input regimes (RS and IS) resulted in a significantly lower average synaptic weights than asynchronous input ($t(48) = 13.32$, $p < 0.001$). Despite these differences, there was no significant difference in the stability of synaptic weight across time as a consequence of input type (coefficient of variation comparisons, $p > 0.2$). The distribution of excitatory synaptic weights was also similar across all simulations. Weights tended to cluster near maximal and minimal values. This pattern is typical of networks where an additive STDP learning rule is applied (Song et al, 2000). Fig 4 shows example weight distributions at the end of simulations for each input regime. Since the STDP rule was only applied at RSE → RSE synapses, weights on inhibitory synapses remained constant.

The average neuronal synaptic degree for excitatory neurons showed a similar pattern to that of the average synaptic weights. In this analysis, only synapses to and from excitatory neurons were counted. For all simulations, the average synaptic degree per excitatory neuron was 46.27 synapses (s.d. = 1.04). The stability of average neuronal degree across time was high (average coefficient of variation across simulations = 0.002; s.d. < 0.001). External input type exerted a significant effect on synaptic degrees ($F(1,4) = 229.79$, $p < 0.001$) where synchronous input regimes resulted in lower average neuronal degrees than asynchronous

regimes ($t(48) = 13.87$, $p < 0.001$). Input type also significantly affected the stability of average neuronal degrees across time (i.e. the average coefficient of variation; $F(1,4) = 11.47$, $p < 0.001$). Networks receiving synchronous input were more stable ($t(48) = 3.92$, $p < 0.001$). The distributions of pre-synaptic connections and post-synaptic connections (the in-degrees and out-degrees, respectively) were highly similar across simulations for a given input type. Fig 5 shows example degree distributions for each input regime.

Small-world topology was also evaluated across the analysis interval. The overall average clustering coefficient for RSE → RSE neurons across the analysis window for all simulations was 0.435 (s.d. = 0.006). In every simulation, the clustering coefficient was greater during the analysis interval than at initialization (mean across all 10 initial networks = 0.3368, s.d. = 0.0022), suggesting increased clustering due to on-going STDP and external input. Clustering coefficients varied little across the analysis interval (coefficient of variation of clustering, mean = 0.004, s.d. < 0.001). Further, clustering was significantly affected by external input type ($F(1,4) = 30.62$, $p < 0.001$), as was the coefficient of variation ($F(1,4) = 10.29$, $p < 0.001$) such that synchronous input decreased clustering ($t(48) = 8.67$, $p = 0.003$) and increased variability ($t(48) = 3.10$, $p = 0.009$). In contrast, the average shortest path length increased almost an order of magnitude over its value at initialization (path length mean at initialization = 0.3537, s.d. < 0.001; mean of overall path length during analysis interval = 3.196, s.d. = 2.03). Path length was also much more variable during the analysis interval as is apparent in by the coefficient of variation across time (mean = 1.91, s.d. = 1.34). Unlike clustering, external input type did not significantly affect path length or its temporal variability.

Three Neuron Subgraphs (Triads) Reveal Local Topological Dynamics

In the ten original random networks formed at initialization, an average of 1,002,498 unique triads were present (s.d. = 7216.74). In general, the number of these triads that remained in each network (i.e. that were detected at least once during the analysis interval) was a small fraction of those present at initialization. The percentage of total triads that remained varied significantly according to input type ($F(1,4) = 275.83$, $p < 0.001$), where synchronous input regimes resulted in significantly smaller percentages of remaining triads ($t(48) = 13.47$, $p < 0.001$).

In all of the simulations, the set of remaining triads was divided between core triads, which showed no change in their connectivity pattern throughout the analysis interval, and dynamic triads, which disappeared, re-emerged, or changed triad type at least once during analysis. The percentages of the core triads and dynamic triads present in each network depended upon the external input type each received ($F(1,4) = 54.52$, $p < 0.001$) such that synchronous input significantly increased the proportion of core triads ($t(48) = 9.31$, $p < 0.001$).Table II displays demographics for the core and dynamic triads for each input regime.

Core Triads Consist of Strong and Stable Synapses

The strength and stability of core triads were determined by assessing their triad intensities and coherences. Core triad intensities from all simulations approached maximal values (overall mean = 7.99 mV) as did core triad coherences in all simulations (overall mean > 0.999). The high values of core intensities and coherences suggest that these triads consisted of strong, symmetric synapses. The values of intensities and coherences from all of the simulations were very similar (overall s.d., intensity = 0.005; s.d., coherence < 0.001). Nevertheless, a significant effect of external input type was detected (intensity, $F(1,4) =$

221.61; coherence, $F(1,4) = 7.68$; $p < 0.001$ both). Regular regimes reduced the coherences of core triads ($t(48) = 2.46$, $p = 0.017$) while synchronous regimes slightly increased both core intensities ($t(48) = 14.26$, $p < 0.001$) and core coherences ($t(48) = 3.33$, $p = 0.002$).

Fig 6 and Table III display the distributions of the different types of core triads averaged across the different input regimes. Two-synapse core triad types (types 1, 2, and 3) occurred in every simulation, as did core triads of type 5. Type 7 core triads were observed in several of the simulations involving asynchronous input (IS, IA50, IA12). No other core triad types were observed in any of the simulations.

Dynamic Triads Enhance the Diversity of Local Topologies

Dynamic triads are those triads which were detected during analysis but which changed connectivity pattern at least once during the analysis interval. Whereas synchrony significantly increased the proportion of core triads observed, asynchronous input increased the proportion of dynamic triads.

Example distributions of the average intensities and coherences of dynamic triad types for each external input regime are shown in Fig 7. Intensities and coherences from all simulations displayed a bimodal and skewed distribution. The bimodal and negatively skewed distributions suggests that a large proportion of these triads possessed relatively strong, stable synapses despite on-going state changes while a smaller proportion were more unstable. Alternatively, this distribution pattern may reflect high frequencies of individual triads which possessed both strong-stable, and weak-unstable states. The intensities and coherences of synapses forming dynamic triads varied according to input type (intensity, $F(1,4) = 34.84$; coherence, $F(1,4) = 28.58$; $p < 0.001$ both). Similar to core triads, regular input regimes (RS, RA) significantly reduced both the intensity ($t(48) = 2.72$, $p = 0.009$) and

coherence ($t(48) = 3.18$, $p = 0.003$) of dynamic triads. Synchronous input significantly increased both measures (intensity, $t(48) = 4.98$; coherence, $t(48) = 4.11$; $p < 0.001$ both).

The number of state changes, the repertoire sizes, and the durations of each dynamic triad were also evaluated. All of these measures were influenced by the external input that the network received. The average number of state changes across all simulations was 7.74 changes (s.d. = 0.795 changes) per triad and depended on external stimulus type ($F(1,4) = 49.57$, $p < 0.001$) such that synchronous input significantly reduced the number of changes ($t(48) = 8.46$, $p < 0.001$). Some dynamic triads consisting of more than two synapses could appear as multiple triad types during the analysis interval. The repertoire sizes and triad durations were quantified for all dynamic triads in the network under each of the separate input regimes. The majority of triad types in the networks were composed of two synapses (types 1, 2, and 3), and dynamic triads of this type could only exist in two states (either as non-triads or as the original triad type). Therefore, the overall distribution of triad repertoires was heavily skewed toward single triad repertoires. The average repertoire size of the dynamic triads was 1.13 types (s.d., 0.15 types), and the average triad duration was 44.35 % (s.d., 1.47 %). Similar to the number of state changes, both the repertoire sizes and triad durations were influenced by input regime (repertoire size, $F(1,4) = 72.09$; duration $F(1,4) = 22.36$; $p < 0.001$ both). Synchronous regimes significantly reduced repertoire sizes ($t(48) = 11.17$, $p < 0.001$) and regular input regimes significantly increased triad durations ($t(48) = 8.36$, $p < 0.001$).

Similar to core triad distributions, dynamic triad types consisting of two synapses (types 1, 2, and 3) and triad type 5 occurred most frequently; however, dynamic triads were more diverse and all triad types were detected at least once during the simulations. Because

dynamic triads can change type, distributions represent the average number of types across the analysis interval rather than sums of individual triads. Despite the dynamic range of these triads, the distribution of triad types remained highly stable across time (overall coefficient of variation across all triad types = 0.865). Fig 6 displays the distributions of dynamic triad types and Table III displays means and coefficients of variation.

To fully assess the dynamics of the local topology, the numbers of individual triads which disappeared and re-emerged across each sampling interval was calculated. The average number of individual triads which were lost from one sampling point to the next was 15459.25 (s.d. = 3765.55), while the number that were gained (re-emerging as either as the same type or as a different type) was 15444.37 (s.d. = 3762.79). Interestingly, nearly as many triads were gained as lost at each timepoint, keeping the overall number of triads across time negligible. For all simulations, the average change in the total number of triads from one sampling point to the next was +/- 1676.47 triads (s.d. = +/- 378.78). To better quantify the disparity between the numbers of individual triads which disappeared and re-emerged and the overall changes in triad counts, the ratio of the number of triads which re-appeared at each sampling point to the absolute net change in triad counts was calculated. The overall gained-to-net ratio was 9.26 (s.d. = 1.54) across all simulations, almost a tenfold increase. This implies that the total number of triads (and the distribution of triad types) barely changed while the composition of participating triads was changing at nearly ten times the rate. External stimulus type influenced triad losses, gains, net changes, and gained-to-net ratios ($F(1,4) = 275.68$, 275.22, 35.64, and 7.61, respectively; $p < 0.001$, all cases). In every case, synchronous input significantly reduced these values ($t(48) = 13.09$, 13.06, 6.79, and 2.95, respectively; $p < 0.001$ for first three measures; $p = 0.005$ for gain-to-net ratio). Fig 8 and

Table IV display the average number of individual triads that were gained and lost at each sampling point, as well as net changes in total number of triads.

The Final Networks Possess Significant Motif Types

When specific triad types occur more frequently than would occur by chance, they are considered to be significant motifs. Triad type distributions were monitored throughout the analysis interval, and the types present in the final networks were subjected to motif analysis. Table V displays the number of significant triad types (motifs) found in the final networks for each input regime. In every simulation, triad types 2 and 5 were found to be significant motifs, occurring more frequently than in random networks. Triad type 8 also occurred significantly more frequently across all input regimes. Triad types 1, 3, and 7 occurred significantly less frequently in all simulations, while types 4, 6, 10 and 11 occurred significantly more in some simulations and significantly less in others depending on the type of external input the networks received.

Variations in STDP Learning Parameters and Network Configurations Have Mixed Effects on Stability and Dynamics

Several changes were made to STDP and network parameters to evaluate their effects on topological stability and dynamics. To this end, networks employing parameter variations were directly compared to standard networks on the coefficients of variation of global variables across time, on percentages of core triads and dynamic triads, and on the gained-to-net ratios of triads. All of these measures are dimensionless and are thus suitable for comparisons across networks where quantitative differences are likely to occur. Further, they capture qualities of topological change that direct comparisons of means may not. Tables VI

and VII report values of topological features obtained from each parameter variation condition.

Overall, each of the STDP rule modifications had only marginal effects on network stability. The global measures remained highly stable across time in each condition (mean coefficient of variation across all measures = 0.002; s.d. = 0.002), comparable to the stability seen in these measures in the original simulations. Nevertheless, the reduced STDP window condition resulted in a significant decrease in neuronal degree variability across time when compared to the original simulations (coefficient of variation of neuronal degree; $t(9) \leq -3.35$, $p \leq 0.01$).

The largest differences observed from the STDP modified simulations were in the percentages of core and dynamic triads. The proportion of core-to-dynamic triads was significantly increased in almost every simulation involving an STDP parameter modification ($t(9) \geq 3.35$, $p \leq 0.01$), indicating that the composition of core and dynamic triads remaining in the network was sensitive to changes in STDP potency.

The gained-to-net ratios of triads across time were significantly reduced by the symmetric STDP condition during exposure to asynchronous input regimes (IS, IA50, IA12) and by the reduced STDP window condition during RA stimulation ($t(9) \leq -3.35$, $p \leq 0.01$); however, the ratios still remained high in the STDP modification conditions, suggesting that large ratios is a robust effect.

Changes in network configuration parameters included a reduced synaptic weight condition, an asymmetric weight condition, a sparse connectivity condition, and a stationary input layer condition.

In the reduced synaptic weight condition, global measures remained highly stable across time; however, significant increases in the coefficients of variation of the average weights and number of synapses were observed when compared to networks with the original weight range ($t(9) \geq 3.35$, $p \leq 0.01$). In every simulation involving the reduced weight condition, percentages of the core triads were reduced ($t(9) \leq -3.35$, $p \leq 0.01$). This effect was so great in the IA50 and IA12 simulations that no core triads were observed during the analysis interval. An effect of this parameter variation was also observed in the triad turn-over rates. This condition significantly increased gained-to-net ratios in almost all simulations ($t(9) \geq -3.35$, $p \leq 0.01$), sometimes achieving values of over 30 triads gained for each net change in triad count.

The asymmetric weight condition did not significantly alter the temporal stability of any of the global measures with the exception of an increase in the coefficient of variation of the number of synapses during the IA12 input regime ($t(9) \geq 3.35$, $p \leq 0.01$). Additionally, the core-to-dynamic triad ratio was significantly reduced following RA input ($t(9) \leq -3.35$, $p \leq 0.01$); however, all other input types resulted in increases in the ratio ($t(9) \geq 3.35$, $p \leq 0.01$). The gained-to-net ratio of triads decreased in this network in every input regime except during RS input. Nevertheless, values remained high, suggesting that substantial triad turn-over continued to occur.

Reducing network connectivity resulted in several significant differences. Although they remained low, the sparse connectivity condition increased the coefficients of variation of all of the global measures (decreased global network stability) in almost all of the simulations ($t(9) \geq 3.35$, $p \leq 0.01$). This condition also significantly decreased the core-to-dynamic triad ratios in every simulation ($t(9) \leq -3.35$, $p \leq 0.01$). Effects of sparse connectivity on gained-to-

net ratios varied according to input regime: RA, RS, and IS input decreased the ratio while IA12 input increased the ratio ($t(9) \leq -3.35$; $t(9) \geq 3.35$; $p \leq 0.01$, all).

During the stationary input condition, global stability was not significantly altered except for an increase in the stability of the average neuronal degree across time (i.e. decreased coefficient of variation of degree; $t(9) \leq -3.35$, $p \leq 0.01$). This condition also significantly increased the core-to-dynamic triad ratios in all simulations ($t(9) \geq 3.35$, $p \leq 0.01$). The gained-to-net triad change ratio was also decreased in every simulation ($t(9) \leq -3.35$, $p \leq 0.01$).

Qualitative comparisons between triad type distributions from parameter modified networks and standard networks suggest that these modifications did not substantially alter the distributions of different triad types. Coefficients of variation of the 13 types across time were marginal (mean coefficient of variation across types = 0.707) and comparable to those from the unaltered simulations, indicating a stable distribution across time.

Chapter 4

Discussion

Previous theoretical and empirical work has demonstrated that STDP is capable of selecting unique and presumably advantageous topological features, such as small-world properties and specific mosaics of motifs (Shin and Kim, 2006; Ren et al., 2009). This report demonstrates that not only does STDP select these features, but it also maintains them across a broad range of input regimes and parameter values. The low variability in measures such as synapse count, clustering, degree distributions and frequencies of motif types across time reveals that STDP-driven networks are highly stable even in the presence of noisy and unpredictable input. However, this global stability belies a dynamic local topology which remains flexible and responsive. This balance of stability and flexibility is critical for unsupervised learning and underscores the viability of STDP as a powerful tool not only during neurobiological development but throughout the lifespan.

One of the key features of the evolving STDP networks examined was the presence of both persistent core triads and transient dynamic triads. Because the proportions of core and dynamic triads varied considerably under different input regimes, both presumably play a role in network responses to external input. Core triads were composed of strong and stable synapses, similar to a pattern that has been observed *in vitro*. Song et al., (2005) found a core network of strongly connected triads among layer V neurons in rat visual cortex. The authors described this local cortical network structure as "a skeleton of stronger connections in a sea of weaker ones." Although speculative, they suggest that these triads drive network activity and are responsible for the stereotypical firing patterns observed in cortical slices. Consistent with this hypothesis was the occurrence of more consistent firing activity patterns in

networks which received synchronous input. Synchronous regimes increased triad strength and stability and resulted in networks of more core triads. Dynamic triads were less dynamic, as evidenced by reduced numbers of state changes and repertoire sizes, and increased durations in the network. Consequently, the turn-over in triad participation was also reduced. Asynchronous input had opposite effects. It would appear that synchrony promotes networks composed of fewer but stronger and more stable triads. One might speculate that this occurs because synchronous input results in fewer but stronger synapses. However, this is not the case. Synchronous input had no significant effect on the number of synapses in the network and actually resulted in significantly lower synaptic weights than asynchronous input. This would suggest that the pairing of synchronous external input and STDP operates at the level of the triad rather than the individual synapse. Numerous studies have documented increased synchrony in recurrent networks which employ STDP (e.g. Masuda and Kori, 2007; Takahashi et al., 2009). The presence of core triads in these networks may contribute to this phenomenon. Indeed, Song and colleagues suggested that STDP may be a key mechanism leading to the emergence of a "skeleton" of core triads.

The presence of dynamic triads in these networks may have larger consequences. After exploring a range of brain and neural networks from several species, Sporns and Kotter (2004) proposed a distinction between structural and functional motifs (triads). According to their interpretation, the physical connections between neurons or brain regions form structural motifs and functional motifs are transient activations upon these structural motifs recruited during on-going information processing. Some structural motifs possess a repertoire of functional motifs because distinct subsets of connections can be selectively activated. Motif types composed of more connections, such as type 10, possess larger repertoires

because of the number of functional motifs that can be formed from them. The authors have argued that topologies comprised of a small set of structural motifs with large repertoires of functional motifs are highly efficient because they increase computational capacity with low wiring costs. In the present report, dynamic triads are analogous to the functional motifs that Sporns and Kotter describe. Their presence illustrates how a simple and biologically realistic mechanism, STDP, provides a viable means for recruiting functional motifs to accommodate on-going demands. Further, the set of the functional motifs which are employed at a given moment can be modified by synaptic potentiations and depressions. Since a single synapse invariably participates in a multitude of motifs, subtle changes in the weights of just a few synapses can lead to network-wide changes in motif activity. Thus, STDP increases network efficiency even further by adding another dimension to computational capacity (the mosaic of active functional motifs) with relatively low metabolic costs. The work of Sporns and Kotter primarily addresses motifs formed between different cortical areas rather than between individual neurons. It has been demonstrated that learning can modify features of both structural and functional cortical networks in humans and other species (e.g. Buchel et al., 1999; Mcintosh et al., 2003). It will be interesting to see if STDP or some other mechanism is governing these changes.

Another interesting finding concerns the degree of "small-worldness" observed during the network simulations. The appearance of increased neural clustering coupled with increased distances between neurons suggests a much more localized network than would be expected in a small-world topology. However, the highly dynamic nature of the path lengths during the simulations must be considered. Widely fluctuating distances between neurons throughout the analysis interval suggests that there were moments of greater small-worldness

intermixed with moments of more localization and restriction. Here, distance is not merely interpreted by the number of synapses between neurons but also reflects the strengths of the synapses separating them. In this case, a path formed by several strong synapses may be of more advantage than a path consisting of a single weak synapse. Again, STDP may enhance the functional capacity of these networks by varying the strengths of key synapses rather than through forming new pathways. The modulating path lengths may act as a functional gating mechanism which could significantly enhance the computational properties of network. Incorporating synaptic weights and directionality into the evaluation of path lengths may also explain why this study did not find the emergence of a consistent small-world topology while similar studies did (Suzuki and Ikeguchi, 2005; Shin and Kim, 2006). Indeed, when path lengths were evaluated without consideration of direction or weight in the present simulations, values dropped considerably and practically no temporal variability was observed (unpublished data).

One of the more important findings in this report was the large amount of triad turn-over observed despite negligible changes in the total number of triads or in the distribution of triad types. This scenario is analogous to a busy train terminal. Throughout the day people are busy coming and going, although the total number of people in the station at any given point in time may stay about the same. The make-up of the different types of people in the terminal, for example the number of men, women, and children could also remain constant even though specific people are continuing to arrive and depart. The highly dynamic behavior and shifting participation of individual triads suggests that they may play an important computational role in the networks. As a caveat, researchers should be cautious in

assessing the activity of any complex network without taking into account the unique participations of individual network constituents.

Hinting at a potential role that these triads may play, it should be noted that the patterns of significant motifs detected in the final networks from these simulations were similar to patterns detected by Ren et al., (2009) in similar STDP model networks. This suggests that these motifs may be a general consequence of STDP. Types 5 and 8 were found to occur significantly more frequently in STDP models from both studies (compared to random networks), and type 2 was also significantly more frequent in the simulations presented here. These types have also been found to be significant in the nervous systems of living organisms, such as C. *elegans*, bolstering the claim that these systems may develop in the presence of STDP (Ren et al., 2009). Motif types 2, 5, and 8 are related and belong to a motif "super family" due to their common feed-forward nature (Milo et al., 2004). It has been reasoned that STDP favors the potentiation of feed-forward patterns and discourages circular patterns (like type 7, which occurred significantly less frequently) due to the phasic nature of pre- and post-synaptic firings (Kozloski and Cecchi, 2010). It has also been asserted that this phenomenon underlies the promotion of network synchrony, although not all findings support this claim (e.g. Kunkel et al., 2011). At any rate, the emergence of local feed-forward topologies likely contributes to the ability of STDP to maintain stability in recurrent networks (Diesmann et al., 1999; Reyes, 2003). Although not tested directly, given the extremely low variability in the frequencies of these feed-forward triad types across time and input regimes, it seems reasonable to conclude that their presence remained significant throughout the simulations. It may be the case that STDP is required to actively maintain this topological

profile in the face of on-going, unpredictable input rather than serving to merely "hard-wire" an invariant final topology.

Changes in STDP and network parameters have revealed the robustness of some topological features and the sensitivity of others. Although significant differences did occur because of parameter changes; synaptic numbers, strengths, and neuronal degrees remained highly stable across time and high triad turn-over continued to occur. However, the ratios of core and dynamic triads present in the networks deviated substantially. Decreases in either the number of synapses or their weights resulted in networks with significantly more dynamic triads. This may be a consequence of maintaining the same amount of external input as in the standard simulations. By reducing the number of synapses, input becomes more concentrated and gives STDP more events per synapse to operate upon. Along the same lines, reducing the synaptic weight range while keeping the same learning rate gives STDP more 'bang for its buck' during each synaptic event. With each parameter change, synaptic modification is either more frequent or more pronounced which reduces the number stable synapses available to form core triads. Consistent with this interpretation, when the learning rate was reduced while the weight range remained the same, more core triads emerged, perhaps because each synapse was less sensitive to STDP. Modelers have long known that the difference between the maximal synaptic potential achievable (maximum weight) and the maximum impact a synaptic event can have (learning rate) is an important measure in maintaining network stability. It appears that it is also an important measure in controlling the dynamics of network topology.

Other parameter variations also significantly affected the numbers of core and dynamic triads. Increasing the overall strengths of inhibitory neurons or defining a fixed

layer of input neurons led to increases in the numbers of core triads. Both of these variations are related in that they define an 'elite' set of synapses which have a disproportionate impact on the network. One might surmise that it is these elite synapses which form the core triads; however, some or all of these synapses were inhibitory, and inhibitory synapses were not included in the core triad counts. As with external synchronous input, it may be the case that core triads emerging from these parameter changes are promoting stereotypical network activity, although the underlying mechanisms aren't clear.

One of the important conclusions that may be drawn from this report is that complex networks can appear static at one level of analysis and yet be highly dynamic at another level. The explorations here provide some insight into how to assess evolving neural networks and other types of networks which change over time. It appears that an important and thus far overlooked metric is motif turn-over rates, and perhaps the turn-over rates of other network constituents. The ubiquity and significance of these metrics in other networks remain to be seen.

As with any model, the simulations presented here represent an idealized version of real world phenomena, and it is possible that critical features or parameter values which could profoundly impact the results were inadvertently left out. As such, the results presented will need to be evaluated empirically. In addition, there are a number of outstanding questions that remain to be addressed. For example, inhibitory synapses were not modified in these simulations although it is likely that these synapses change the functionality of triads (Li, 2008). What influence would inhibitory plasticity have? The spike-timing mechanisms at these synapses appear to be governed by different rules than at excitatory synapses (Haas et al., 2006), and unique behaviors occur in predominantly inhibitory networks where STDP is

at play (Fino and Venance, 2010; Fino et al., 2010). Additionally, STDP represents only one form of synaptic modification. The formation of new synapses, fast and transient synaptic changes, on-going synaptic decay, and the role of neuromodulators in plasticity undoubtedly add to the complexity of topological dynamics and bear further investigation. Finally, a number of other metrics and modifications remain to be explored both theoretically and empirically.

Over the past decade, network science has provided a number of insights into an array of complex systems such as social, biological, and technological networks, as well as real and modeled neural and cortical networks. As a consequence, network scientists have developed new ways of approaching complex systems and have uncovered a number of common features shared by many different types of systems. Nevertheless, despite general agreement that the topology of many of these systems continually evolves, only a handful of studies have begun to explore their on-going structural dynamics. New measures and methodologies are being developed to capture the unique properties of evolving graphs (e.g. Acer et al., 2011; Starnini et al., 2012), and a better understanding of the temporal characteristics of specific systems, such as human contact networks and technological networks, is beginning to emerge (Scherrer, et al., 2008; Kim et al., 2012). However, to date, research into the on-going topological dynamics of neural and cortical networks is almost non-existent. In addition, although there is a spate of theoretical and empirical work addressing the functionality of STDP, the role it plays in shaping network organization beyond early development is underexplored. Hopefully, this work sheds light onto the evolving topology of neural networks and the role that STDP plays shaping and maintaining this topology. It remains to be seen whether the discoveries made here are unique to STDP-

driven neural networks or whether they represent general features of broader classes of complex systems.

Figures

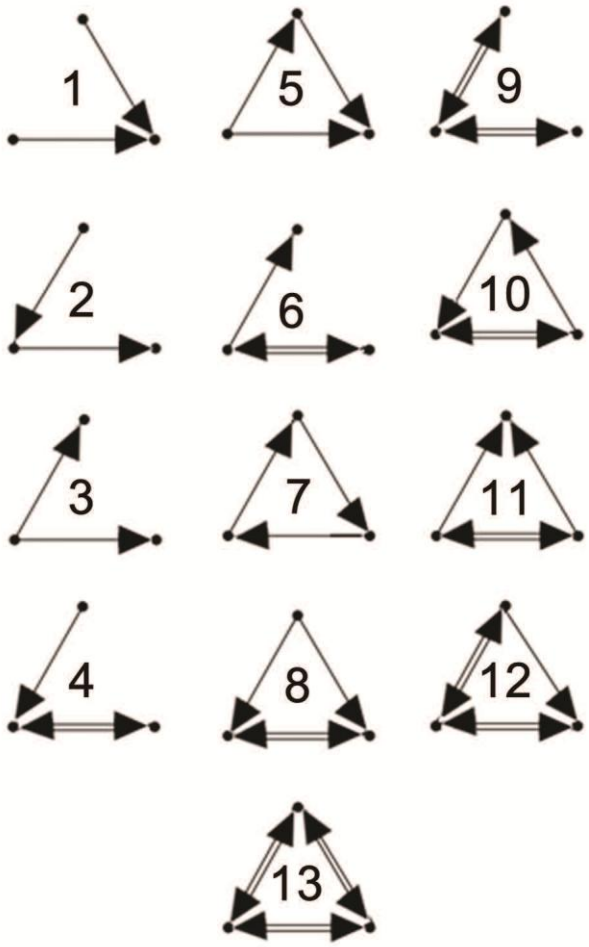

Figure 1 – Triad Types

Configurations of the thirteen possible unique 3-neuron subgraphs (triad types). Numbering scheme taken from Sporns and Kotter, 2004.

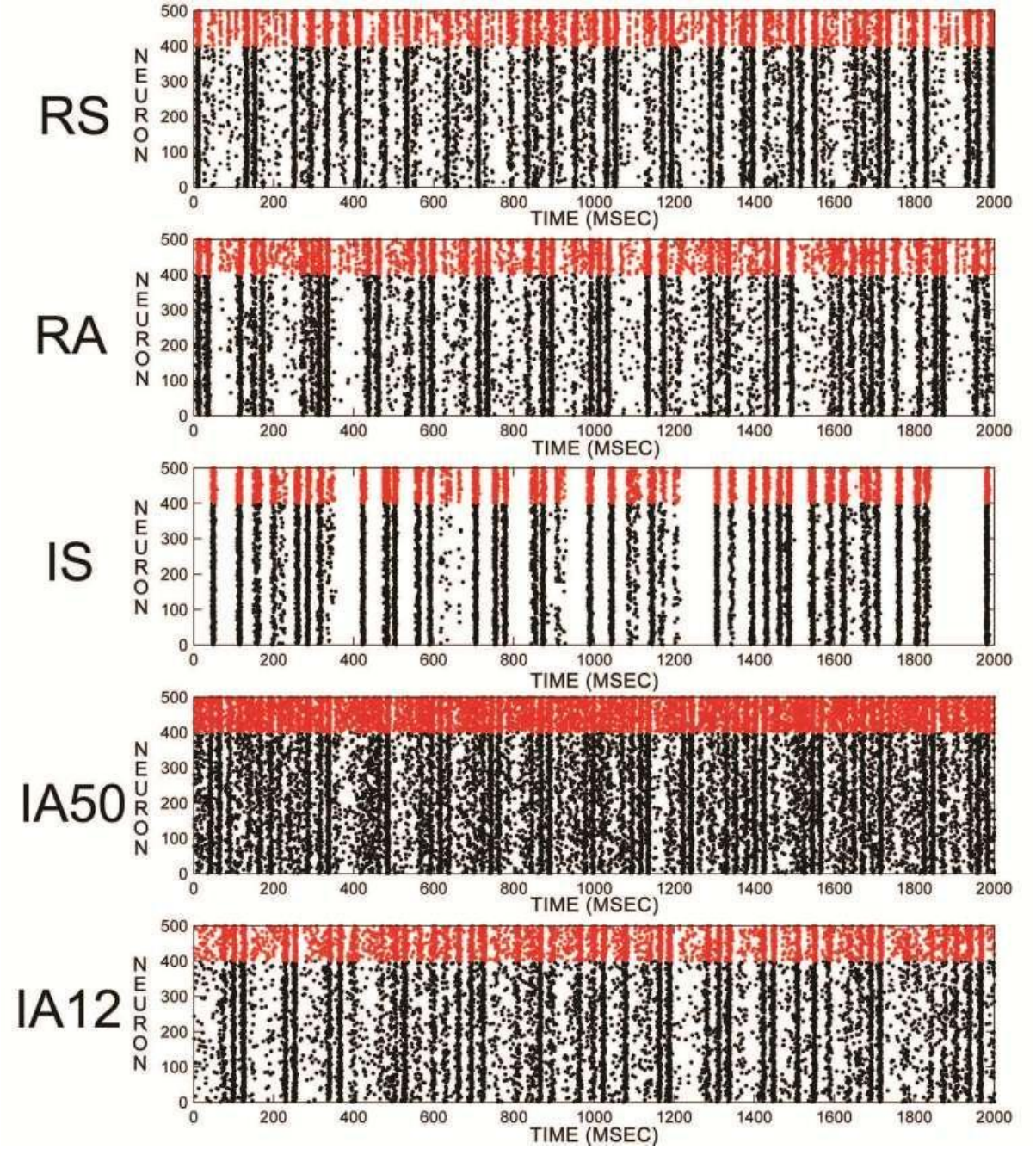

Figure 2 – Network Firing Activity

Exemplar rastergrams of two seconds of network firing activity in response to different input regimes. All examples are from the same initial network. Red datapoints are FSI firings, black datapoints are RSE firings.

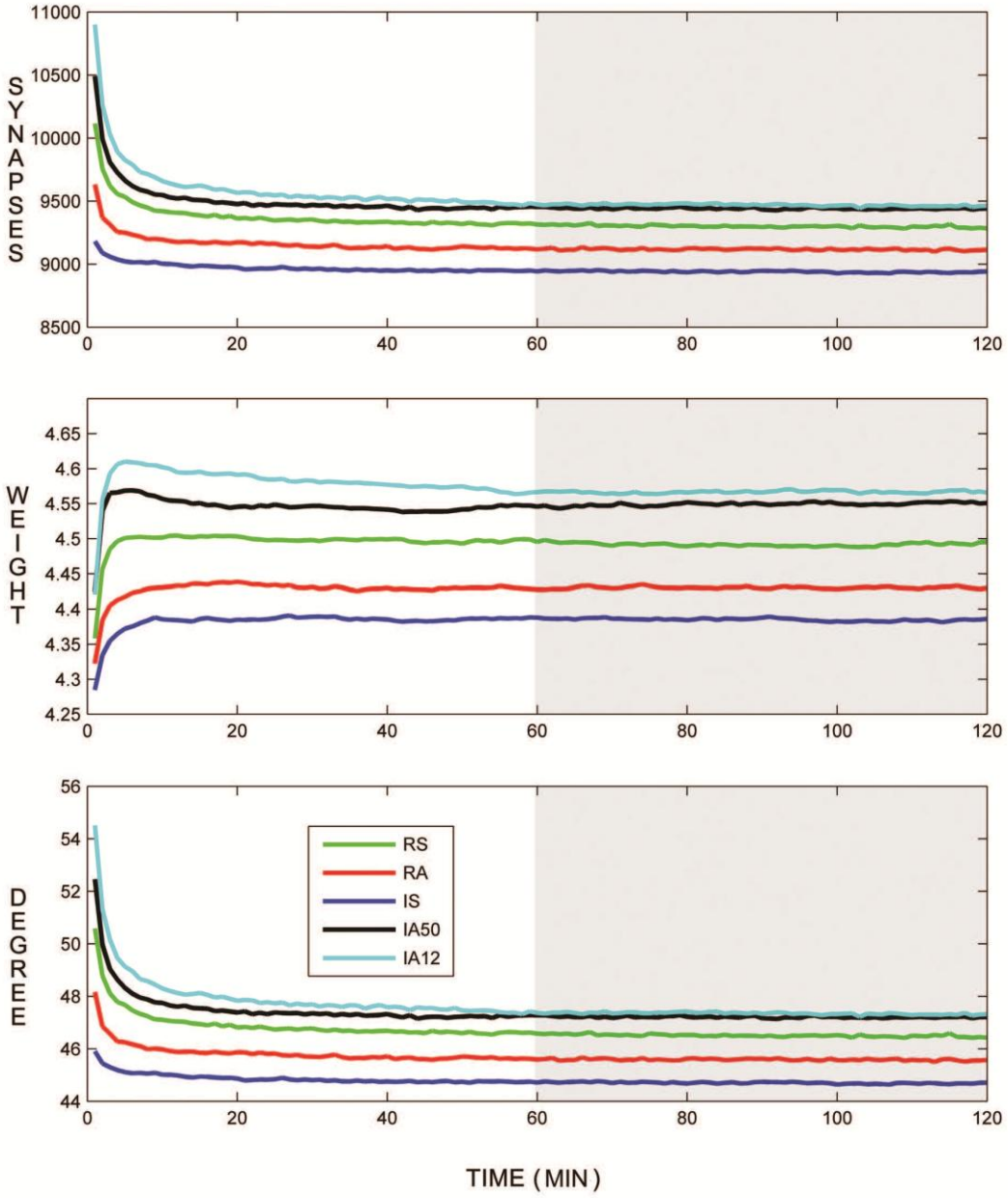

Figure 3 – Global Variables

Trajectories of total number of excitatory synapses (top), average synaptic weight (middle), and average total neuronal degrees (bottom) across the entire simulation duration. Colored lines represent responses to separate external input regimes averaged across 10 simulations. Shaded area represents analysis interval.

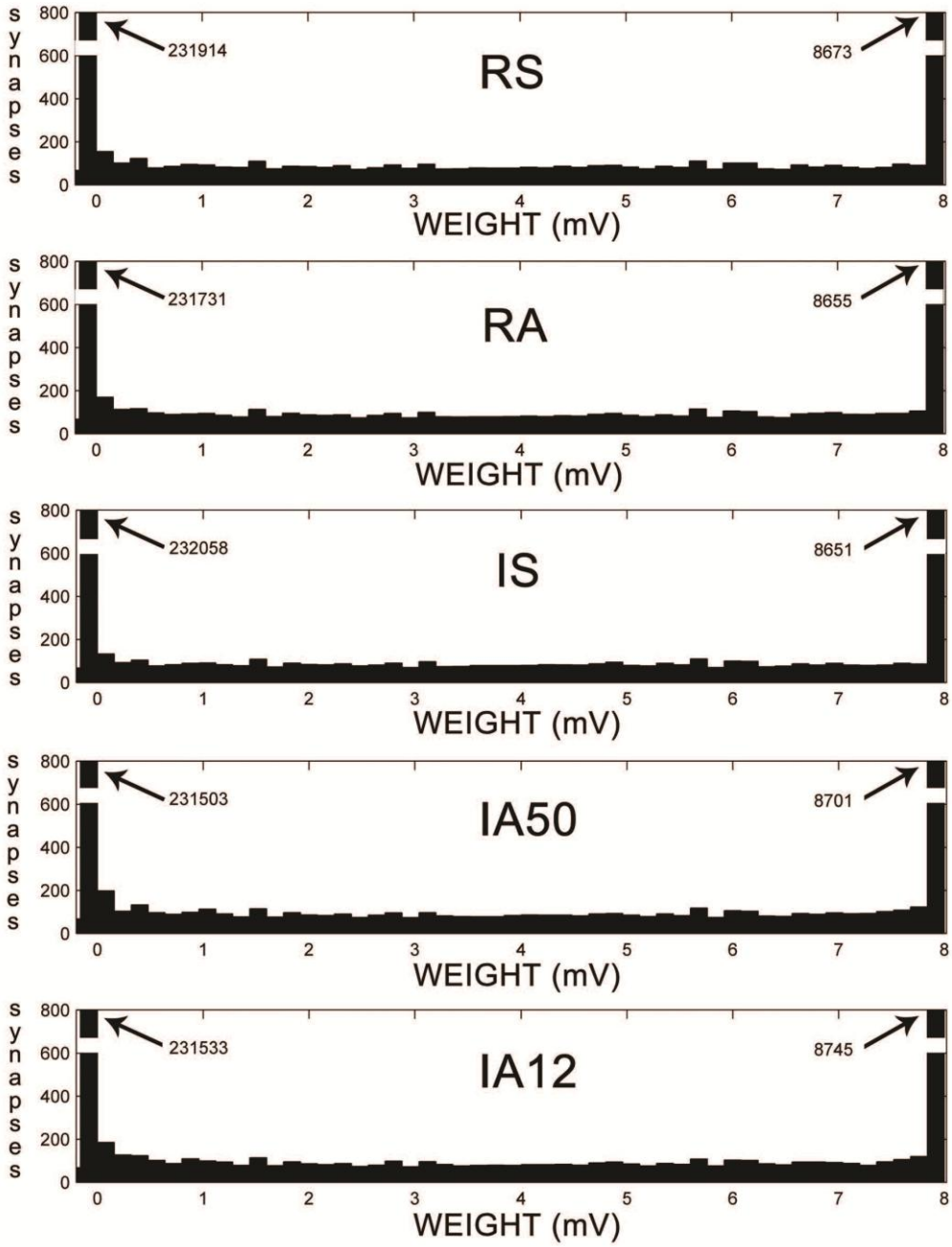

Figure 4 – Final Weight Distributions

Exemplar weight distributions in response to separate external input regimes taken from the last simulation timepoint. All examples are from the same initial network. Bars of the minimum (0 mV) and maximum (8 mV) values are truncated to show intermediate values. Inhibitory weights are not shown.

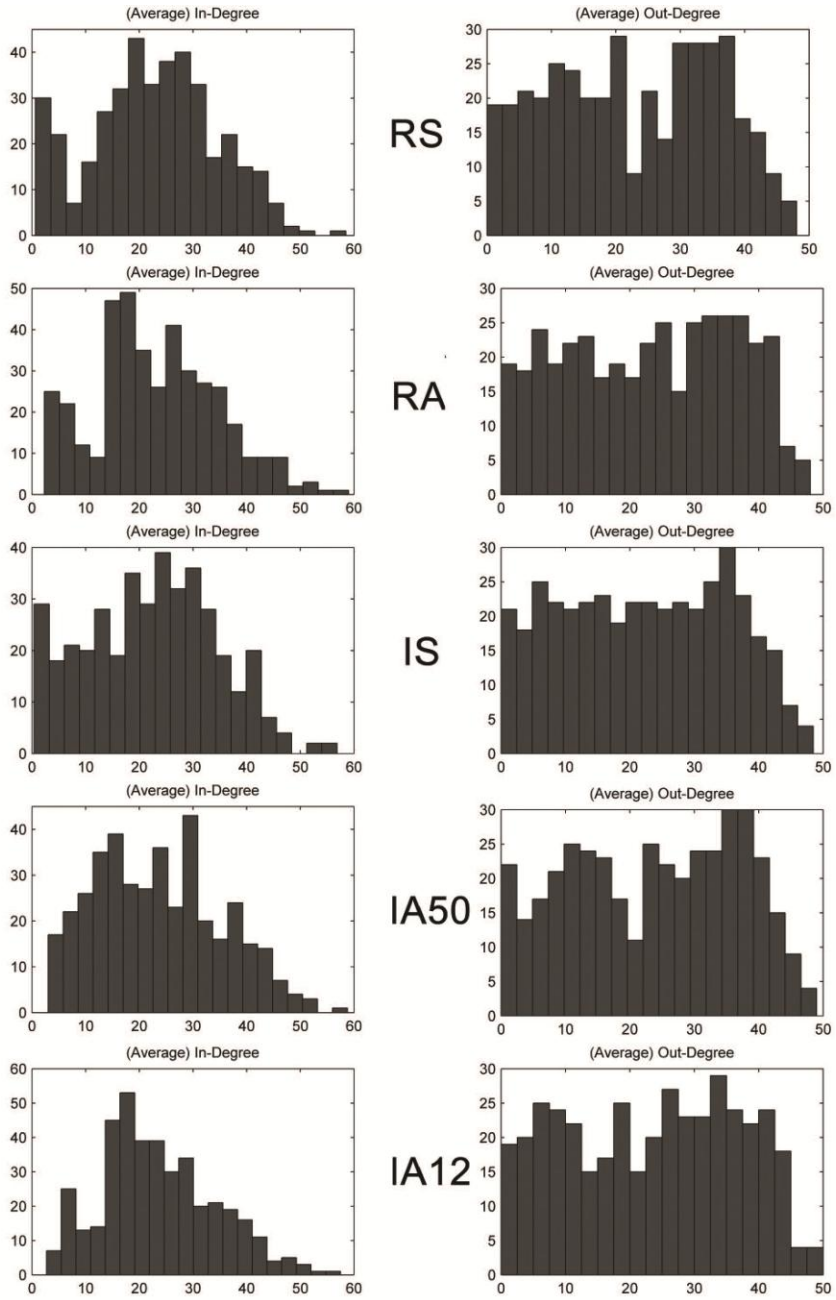

Figure 5 – Degree Distributions

Exemplar in-degree (left) and out-degree (right) distributions in response to separate external input regimes taken from the last simulation timepoint. All examples are from the same initial network. Only RSE → RSE degrees are included. Note that neuron counts (ordinate axes) are not on the same scale for all input regimes.

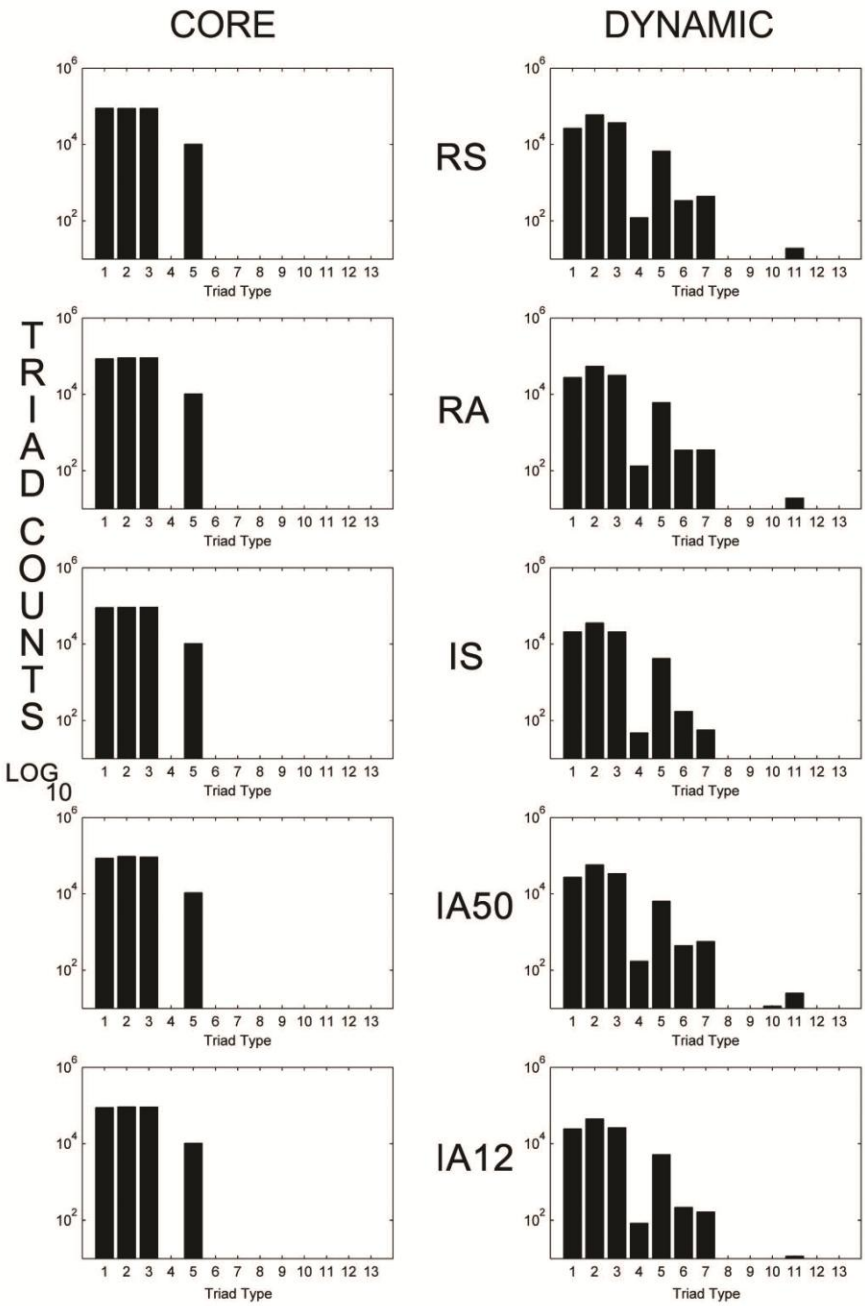

Figure 6 – Core and Dynamic Triad Type Distributions

Triad type distributions for Core (left) and dynamic (right) triads in response to each external input regime averaged across 10 simulations. Dynamic triad distributions are averaged across the analysis interval for each network and then across simulations. Triad counts (ordinate axes) are presented on a logarithmic (base 10) scale. Averages less than one are not shown.

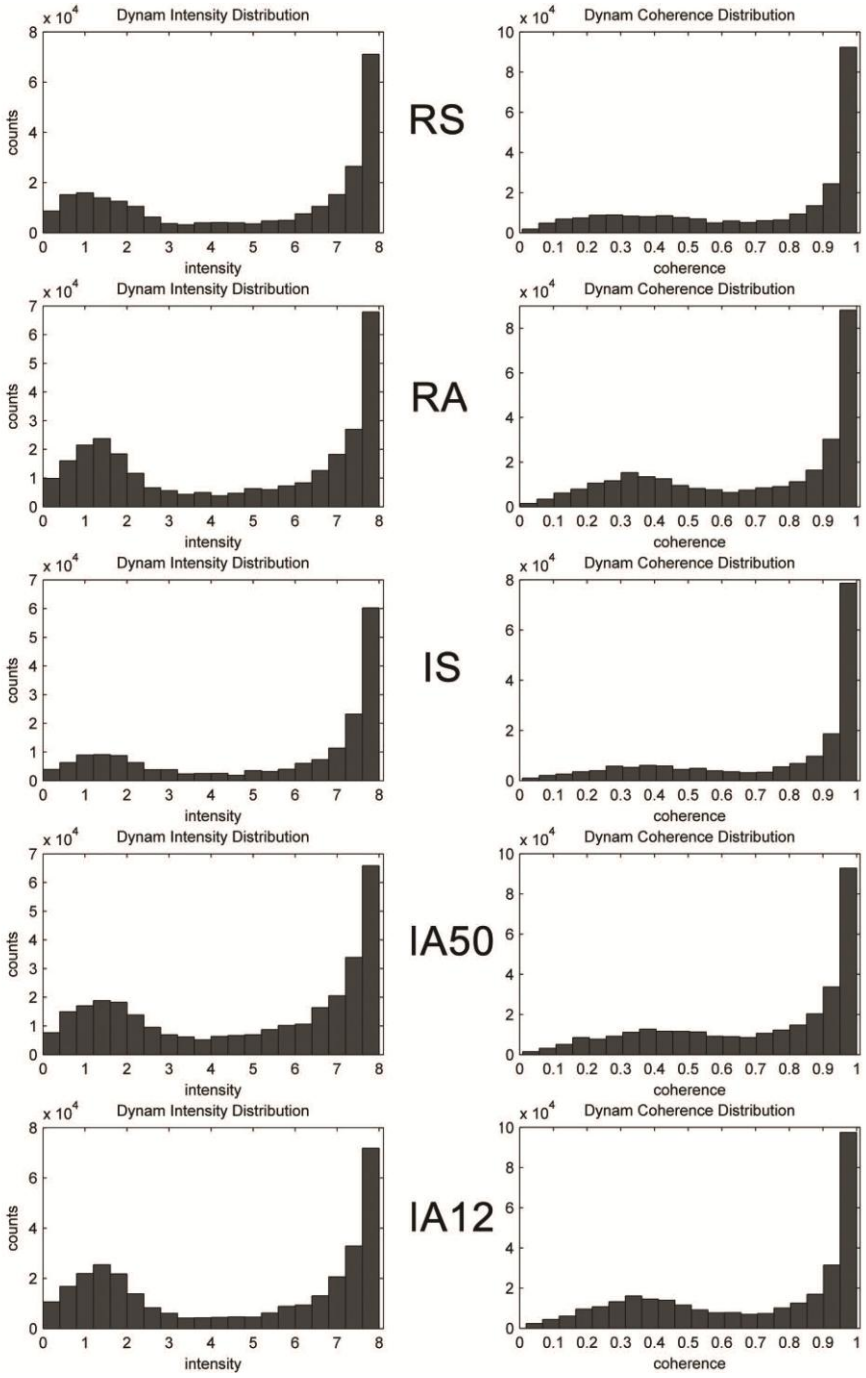

Figure 7 – Dynamic Triad Intensities and Coherences

Exemplar dynamic triad intensity (left) and coherence (right) distributions in response to separate external input regimes. All examples are from the same initial network. Note that triad counts (ordinate axes) are not on the same scale for all input regimes.

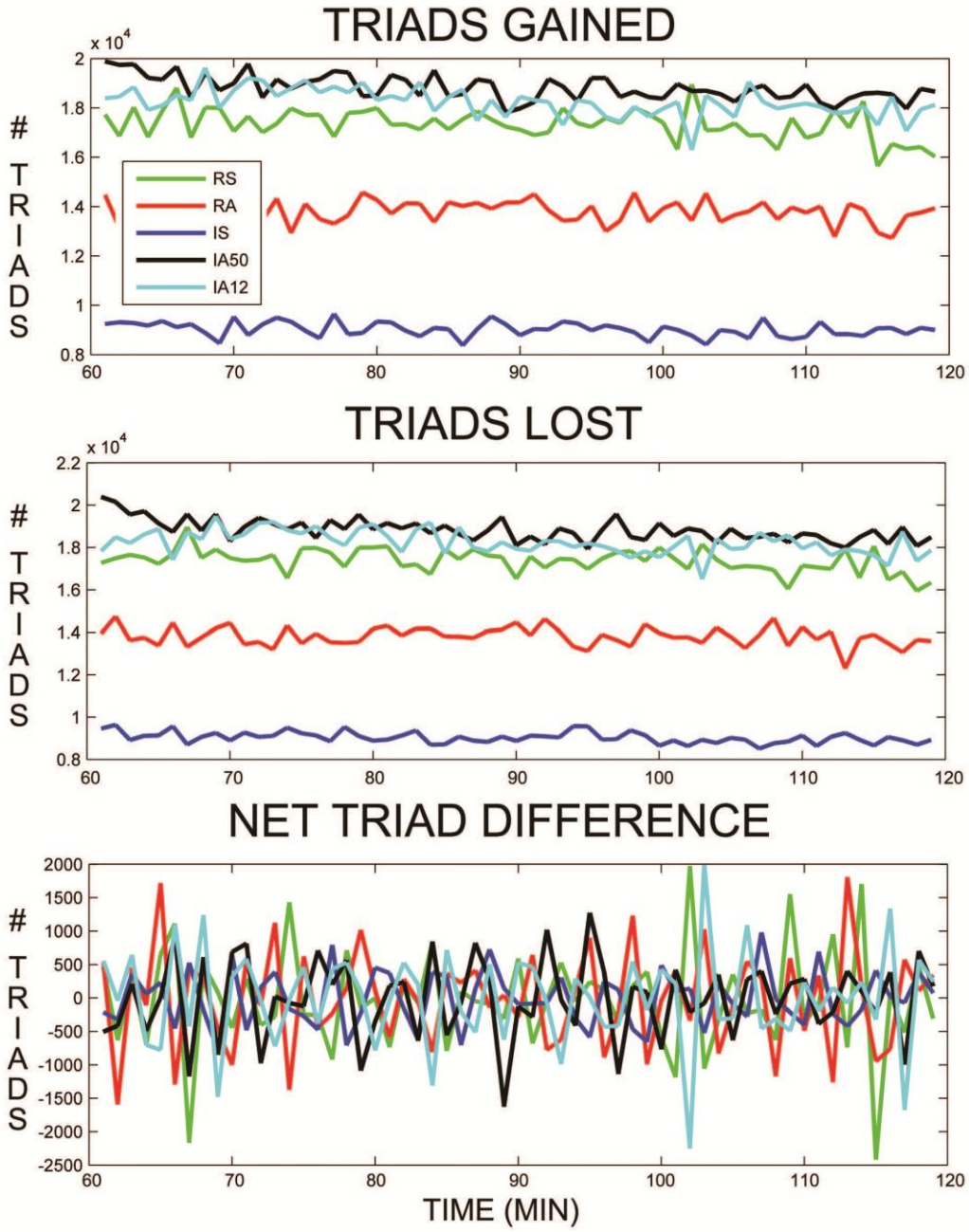

Figure 8 – Dynamic Triad Trajectories

Average number of dynamic triads gained (top), lost (middle) and net triad number differences (bottom) for each minute in the analysis interval. Each minute (abscissa) represents the difference between that minute and the following minute. Colored lines represent responses to separate external input regimes averaged across 10 simulations.

Tables

Table I – Global Variables

	INPUT REGIME				
	RS	**RA**	**IS**	**IA50**	**IA12**
Average Firing Rate	13.64 (0.699,0.205)**	12.89 (0.688,0.232)**	14.51 (0.838,0.134)	15.81 (0.506,0.150)	12.61 (0.672,0.172)
Synapses	9212.23 (20.67,212.22)	9290.67 (23,234.13)	9282.87 (20.73,199.38)	9234.36 (20.78,208.66)	9249.36 (21.49,214.5)
C.V. Synapses	0.0022	0.0025	0.0022	0.0022	0.0023
Synaptic Weight	4.43 (0.006,0.01)**	4.49 (0.008,0.02)	4.39 (0.006,0.02)**	4.55 (0.006,0.02)	4.57 (0.007,0.01)
C.V. Synaptic Weight	0.0014	0.0018	0.0014	0.0014	0.0015
Average Clusering Coefficient	0.43 (0.001,0.003)**	0.436 (0.002,0.004)	0.428 (0.001,0.003)**	0.438 (0.002,0.004)	0.442 (0.002,0.003)
C.V. Clusering Coefficient	0.008*	0.01*	0.007	0.009	0.006
Average Path Length	3.33 (7.76,1.48)	2.61 (5.13,1.11)	4.1 (13.71,3.64)	2.62 (7.38,1.33)	2.56 (6.39,1.46)
C.V. Path Length	2.33	1.97	3.34	2.82	2.49
Average Degree per Neuron	45.59 (0.102,0.21)**	46.5 (0.127,0.22)	44.7 (0.08,0.28)**	47.21 (0.101,0.22)	47.35 (0.124,0.25)
C.V. Degree per Neuron	0.0022**	0.003	0.0018**	0.002	0.003

Values represent means across simulations. Values in parentheses represent s.d.'s across time and networks, respectively.
C.V. is the coefficient of variation (standard deviation / mean) across time.
* indicates significant increase in measure due to input regime
** indicates significant decrease in measure due to input regime

Table II – Triad Demographics

	Input Regime				
	RS	**RA**	**IS**	**IA50**	**IA12**
# of Total Triads	516343.6 (8650.1)*	556875.1 (9821.11)	465299.3 (9944.84)*	566319.7 (10173.93)	569135.4 (9473.55)
% Total Triads	51.51 (0.73)*	55.55 (0.85)	46.41 (0.89)*	56.49 (0.9)	56.77 (0.81)
	CORE TRIADS				
	RS	**RA**	**IS**	**IA50**	**IA12**
% of TTL Triads	54.52 (2.34)*	49.75 (1.95)	61.39 (2.68)*	48.78 (1.95)	50.08 (2.2)
Intensity	7.99 (0.047,< 0.001)*	7.99 (0.064,< 0.001)	7.99 (0.044,< 0.001)*	7.98 (0.061,< 0.001)	7.98 (0.058,< 0.001)
Coherence	1 (0.003,< 0.001)*	1 (0.004,< 0.001)*	1 (0.002,< 0.001)*	0.999 (0.003,< 0.001)	1 (0.003,< 0.001)
% Time as Triad	100	100	100	100	100
Repertiore Size	1	1	1	1	1
State Changes	0	0	0	0	0
	DYNAMIC TRIADS				
	RS	**RA**	**IS**	**IA50**	**IA12**
% of TTL Triads	45.48 (2.34)	50.25 (1.95)*	38.61 (2.68)	51.22 (1.95)*	49.92 (2.2)*
Intensity	4.77 (2.823,0.19)*	4.67 (2.802,0.09)	5.39 (2.798,0.19)*	4.77 (2.828,0.14)	4.7 (2.81,0.17)
Coherence	0.7 (0.303,0.02)*	0.69 (0.298,0.01)	0.76 (0.287,0.02)*	0.71 (0.281,0.01)	0.69 (0.294,0.02)
% Time as Triad	42.94 (35.884,1.14)*	43.01 (35.886,0.6)*	45.69 (35.463,1.08)	45.54 (36.742,0.66)	44.55 (35.903,0.83)
Repertiore Size	1.12 (0.395,0.01)	1.14 (0.423,< 0.001)*	1.11 (0.369,0.01)	1.14 (0.429,0.01)*	1.15 (0.439,< 0.001)*
State Changes	7.53 (6.834,0.42)	8 (6.939,0.24)*	6.45 (6.33,0.33)	8.36 (6.733,0.36)*	8.35 (7.199,0.4)*

Values represent means across simulations. Values in parentheses represent s.d.'s across triads (where appropriate) and/or networks, respectively.
* indicates significant increase in measure due to input regime

Table III – Triad Distributions

TRIAD TYPE	CORE TRIADS				
	INPUT REGIME				
	RS	RA	IS	IA50	IA12
1	87948.9 (2464.055)	85236.1 (2161.244)	90323.9 (2330.471)	89830.5 (1661.41)	85712.4 (2913.244)
2	91914.7 (3663.314)	90907.4 (2941.961)	91879.6 (3532.719)	88042.5 (3070.752)	96123.4 (4002.14)
3	91206.4 (2347.259)	90518.1 (2182.437)	92847.1 (1901.472)	88053.8 (1859.709)	92342.4 (2119.267)
4	0	0	0	0	0
5	10306.4 (356.145)	10248.9 (427.476)	10395.4 (406.427)	10152.6 (310.266)	10702 (432.661)
6	0	0	0	0	0
7	0	0.9 (0.876)	0	0.6 (0.843)	9.6 (3.373)
8	0	0	0	0	0
9	0	0	0	0	0
10	0	0	0	0	0
11	0	0	0	0	0
12	0	0	0	0	0
13	0	0	0	0	0
TRIAD TYPE	**DYNAMIC TRIADS**				
	INPUT REGIME				
	RS	RA	IS	IA50	IA12
1	24486.75 (316.32,2507.193)	27432.17 (414.14,1558.307)	20958.14 (310.11,2685.029)	26692.06 (281.84,2360.944)	27197.09 (362.12,2456.308)
2	44731.36 (849.49,3503.98)	34332.58 (1067.77,2642.003	35859.63 (658.28,3687.466)	60439.94 (893.49,3497.665)	57895.35 (1078.58,3735.6)
3	26097.23 (488.58,1863.52)	31625.32 (573.36,1390.782)	20983.33 (369.87,2109.14)	37402.4 (503.75,1888.146)	33947.03 (617.85,1982.282)
4	84.01 (50.21,16.191)	133.72 (64.12,11.786)	47.16 (35.22,6.366)	121.77 (51.98,19.044)	171.28 (68.14,17.684)
5	5149.22 (100.05,421.378)	6120.18 (123.98,246.43)	4214.36 (83.72,467.738)	6735.49 (103.84,432.454)	6412.09 (123.27,400.931)
6	214.89 (105.32,56.377)	344.51 (139.83,43.572)	171.71 (94,50.253)	340.79 (136.26,49.111)	441.05 (160.92,57.433)
7	162.78 (19.9,21.337)	351.12 (34.74,19.728)	56.53 (9.19,4.703)	442.86 (31.63,26.229)	564.55 (40.12,34.497)
8	4.9 (3.53,0.928)	7.53 (4.39,0.67)	2.61 (2.44,0.301)	6.28 (3.73,0.652)	9.61 (4.84,1.125)
9	0.1 (0.31,0.056)	0.27 (0.57,0.039)	0.06 (0.21,0.071)	0.27 (0.54,0.085)	0.41 (0.69,0.154)
10	2.76 (2.15,0.754)	6.72 (3.88,0.631)	1.03 (1.11,0.253)	7.22 (4.08,0.889)	11.49 (5.54,1.727)
11	11.64 (6.32,3.269)	19.15 (8.71,2.938)	9.6 (6,2.813)	19.22 (8.65,3.016)	25.23 (10.02,3.675)
12	0.01 (0.09,0.015)	0.04 (0.17,0.037)	0.01 (0.07,0.014)	0.03 (0.16,0.024)	0.07 (0.25,0.028)
13	0	0	0	0	0 (0.01,0.005)

Values represent means across simulations. Values in parentheses represent s.d.'s across time (for dynamic triad types) and networks, respectively.

Table IV – Triad Count Change

	INPUT REGIME				
	RS	RA	IS	IA50	IA12
Net Triad Count Change per Min	1623.23 (1249.73,249.12)**	1953.81 (1467.43,146.68)	1087.04 (806.91,85.61)**	1716.94 (1234.55,196.68)	2001.32 (1511.56,240.47)
Number Triads Gained per Min	13802.95 (1373.46,822.98)**	17340.58 (1666.98,858.66)	9025.7 (902.58,459.28)**	18815.17 (1488.23,891.92)	18237.44 (1668.52,778.58)
Number Triads Lost per Min	13811.87 (1283.37,844.65)**	17376.07 (1593.05,868.63)	9035.94 (880.07,441.4)**	18830.03 (1447.61,877.42)	18242.36 (1588.17,770.86)
Gained - to - Net Ratio	8.71 (1.1,1.58)**	8.91 (1.15,0.73)	8.36 (1.12,0.88)**	11.11 (1.21,1.59)	9.23 (1.12,1.16)

Values represent means across simulations. Values in parentheses represent s.d.'s across time and simulations, respectively.
** indicates significant decrease in measure due to input regime

Table V – Significant Motifs

OCCURRED SIGNIFICANTLY MORE													
	Triad Type												
Input Type	1	2	3	4	5*	6	7	8*	9	10	11*	12	13
RS	0	**10**	0	**1**	**10**	0	0	**4**	0	0	0	0	0
RA	0	**10**	0	0	**10**	0	0	**6**	0	0	**1**	0	0
IS	0	**10**	0	0	**10**	**1**	0	**5**	0	0	0	0	0
IA50	0	**10**	0	0	**10**	**1**	0	**4**	0	0	0	0	0
IA12	0	**10**	0	0	**10**	0	0	**6**	0	**1**	0	0	0
OCCURRED SIGNIFICANTLY LESS													
	Triad Type												
Input Type	1*	2	3*	4	5	6	7*	8	9	10	11	12	13
RS	**10**	0	**10**	0	0	0	**10**	0	0	**2**	0	0	0
RA	**10**	0	**10**	**5**	0	**1**	**10**	0	0	0	0	0	0
IS	**10**	0	**10**	0	0	0	**10**	0	0	0	0	0	0
IA50	**10**	0	**10**	**1**	0	0	**10**	0	0	**3**	**1**	0	0
IA12	**10**	0	**10**	**4**	0	0	**10**	0	0	0	0	0	0

Individual cells represent number of simulations in which significance occurred. Ten simulations for each input type.
Types Highlighted in red were significant in all simulations.
* indicates motif types that were found to be significant in STDP models from Ren et al., 2010.

Table VI – Parameter Variation Global Variables

STDP PARAMETER VARIATIONS								
		Global Stability			Triad Dynamics			
CONDITION	Input	C.V. # Syns	C.V. Ave. Weight	C.V. Degree	Change / Min.	Gained / Min.	Lost / Min.	Gained / Net
Reduced Rate	RS	0.0025	0.0005	0.0025	1741.53	13425.65	13406.05	7.7091
Reduced Window	RS	0.0015	0.0011	0.0015	1012.09	8032.56	8005.86	7.9366
Symmetric STDP	RS	0.0024	0.0018	0.0024	1493.85	10923.51	10876	7.3123
Reduced Rate	RA	0.0032*	0.0004**	0.0032	2140.07	17159.59	17231.56	8.0182**
Reduced Window	RA	0.0018	0.0011	0.0018	1431.46	11126.53	11078.49	7.7729**
Symmetric STDP	RA	0.0023	0.0011	0.0023	1683.24	14153.95	14066.65	8.4088
Reduced Rate	IS	0.0015	0.0007	0.0014	1153.92	9159.97	9161.65	7.9382
Reduced Window	IS	0.0015	0.0009	0.0015	950.02	7322.75	7318.39	7.708
Symmetric STDP	IS	0.0018	0.0013	0.0018	1211.92	7569.25	7551.88	6.2457**
Reduced Rate	IA50	0.003	0.0007	0.003	2113.29	18946.13	19014.98	8.9652**
Reduced Window	IA50	0.0017	0.0013	0.0017	1113.53	10964.31	10984.68	9.8465
Symmetric STDP	IA50	0.0018	0.0013	0.0018	1497.17	13115.8	13133.37	8.7604**
Reduced Rate	IA12	0.0029	0.0009	0.0029**	2181.02	19180.83	19248.15	8.7944
Reduced Window	IA12	0.0026	0.0013	0.0026	1603.1	13929.24	14045.97	8.6889
Symmetric STDP	IA12	0.002	0.0013	0.002	1936.32	14750.08	14709.53	7.6176**

NETWORK PARAMETER VARIATIONS								
		Global Stability			Triad Dynamics			
CONDITION	Input	C.V. # Syns	C.V. Ave. Weight	C.V. Degree	Change / Min.	Gained / Min.	Lost / Min.	Gained / Net
Reduced Weight	RS	0.0032*	0.0033*	0.0032*	3374.46	85382.1	85395.51	25.3025*
Asymmetic Weight	RS	0.0023	0.0011	0.0023	1586.63	13208.95	13283.31	8.3252
Sparse	RS	0.0064*	0.0035*	0.0064*	1940.37	13669.17	13673.95	7.0446**
Stationary Input	RS	0.0016	0.0012	0.0016	703.93	3763.03	3730.49	5.3457**
Reduced Weight	RA	0.0033*	0.0047*	0.0033	3984.73	141100.59	140983.25	35.4103*
Asymmetic Weight	RA	0.0029	0.0018	0.0029	2241.7	16864	16826.71	7.5229**
Sparse	RA	0.0058*	0.0038*	0.0058*	2254.03	14758.46	14768.49	6.5476**
Stationary Input	RA	0.0015	0.0012	0.0015**	1092.25	6752.48	6764.09	6.1821**
Reduced Weight	IS	0.0092*	0.0038*	0.0092*	7546.39	68970.17	68842.42	9.1395
Asymmetic Weight	IS	0.002	0.0014	0.002	1217.88	8640.75	8645.17	7.0949**
Sparse	IS	0.0056*	0.0046*	0.0056*	1138.66	7937.2	7888.78	6.9706**
Stationary Input	IS	0.0017	0.0012	0.0017	536.42	2427.78	2414.2	4.5259**
Reduced Weight	IA50	0.0042*	0.0063*	0.0042*	4976.66	194756.25	194647.86	39.1339*
Asymmetic Weight	IA50	0.0025	0.0016	0.0025	2229.73	18842.02	18817.85	8.4504**
Sparse	IA50	0.0044*	0.004*	0.0044*	1835.63	21273.37	21307.92	11.5892
Stationary Input	IA50	0.0023	0.0016	0.0023	1319.29	10783.39	10759.42	8.1736**
Reduced Weight	IA12	0.0038*	0.006*	0.0038	5748.78	169349.36	169372.55	29.4583*
Asymmetic Weight	IA12	0.00338*	0.0013	0.0033	2697.68	18182.61	18186.25	6.7401**
Sparse	IA12	0.0055*	0.003	0.0055*	1328.09	16124.86	16087.73	12.1414*
Stationary Input	IA12	0.0026	0.0016	0.0026	1627.37	12137.78	12154.85	7.4585**

* indicates significant increase in value due to variation ($t \geq 3.25$).
** indicates significant decrease in value due to variation ($t \leq -3.25$).
Note: Triad change per min, gained per min, and lost per min are reported for comparison only and were not tested for significant differences.

Table VII – Parameter Variation Triad Demographics

STDP PARAMETER VARIATIONS											
CONDITION	INPUT	% REMAIN	% CORE	CORE INTENS.	CORE COHER.	% DYNAM	DYNAM INTENS	DYNAM COHER	% TIME	REPERTOIRE	CHANGES
Reduced Rate	RS	48.968	69.583*	7.99	1	30.417	1.697	0.31	30.092	1.122	11.639
Reduced Window	RS	45.794	68.247*	7.995	1	31.753	4.623	0.668	41.164	1.116	7.06
Symmetric STDP	RS	51.409	58.819*	7.991	1	41.181	5.005	0.718	44.758	1.155	6.767
Reduced Rate	RA	53.484	63.952*	7.986	0.999	36.048	1.974	0.35	33.523	1.151	11.617
Reduced Window	RA	51.159	60.884*	7.992	1	39.116	4.467	0.651	39.684	1.126	7.157
Symmetric STDP	RA	53.735	57.772*	7.989	1	42.228	4.731	0.693	44.593	1.159	8.143
Reduced Rate	IS	44.063	75.295*	7.994	1	24.705	2.47	0.395	35.32	1.118	10.809
Reduced Window	IS	44.074	70.546*	7.995	1	29.454	4.888	0.702	43.45	1.105	7.206
Symmetric STDP	IS	47.276	63.807	7.994	1	36.193	5.669	0.78	47.513	1.121	5.715
Reduced Rate	IA50	55.817	64.173*	7.99	1	35.827	1.738	0.324	31.48	1.14	12.308
Reduced Window	IA50	51.893	61.96*	7.993	1	38.04	4.594	0.669	40.275	1.117	7.126
Symmetric STDP	IA50	55.127	56.818*	7.989	1	43.182	5.144	0.737	46.833	1.163	7.298
Reduced Rate	IA12	55.733	62.738*	7.986	0.999	37.262	1.947	0.346	34.845	1.159	12.122
Reduced Window	IA12	54.32	56.463*	7.991	1	43.537	4.527	0.662	41.772	1.148	7.671
Symmetric STDP	IA12	55.933	55.349*	7.987	1	44.651	4.919	0.713	46.274	1.167	7.831

NETWORK PARAMETER VARIATIONS											
CONDITION	INPUT	% REMAIN	% CORE	CORE INTENS.	CORE COHER.	% DYNAM	DYNAM INTENS	DYNAM COHER	% TIME	REPERTOIRE	CHANGES
Reduced Weight	RS	95.059	12.962**	3.95	0.997	87.038*	1.795	0.665	45.102	1.232	13.794
Asymmetic Weight	RS	50.251	57.015*	7.991	1	42.985**	4.622	0.684	43.27	1.124	7.869
Sparse	RS	80.019	27.897**	7.901	0.997	72.103*	4.841	0.745	54.651	1.109	10.717
Stationary Input	RS	36.129	82.943*	7.95	0.997	17.057**	4.848	0.715	44.694	1.108	7.809
Reduced Weight	RA	99.995	3.779**	3.828	0.989	96.221*	2.061	0.765	63.757	1.339	20.33
Asymmetic Weight	RA	55.443	47.616**	7.987	1	52.384*	4.924	0.716	44.001	1.138	7.474
Sparse	RA	79.937	25.908**	7.883	0.996	74.092*	5.325	0.795	61.421	1.114	11.312
Stationary Input	RA	39.878	69.582*	7.918	0.996	30.418**	5.523	0.781	49.711	1.124	7.214
Reduced Weight	IS	86.906	11.026**	3.95	0.996	88.974*	2.111	0.712	44.13	1.234	11.956
Asymmetic Weight	IS	46.403	59.937*	7.993	1	40.063**	5.485	0.763	45.574	1.116	5.954
Sparse	IS	67.277	36.371**	7.976	0.999	63.629*	3.991	0.633	36.915	1.075	8.219
Stationary Input	IS	34.629	84.903*	7.985	0.999	15.097**	5.675	0.793	47.988	1.11	5.918
Reduced Weight	IA50	100	0**	-	-	100*	2.173	0.804	62.65	1.417	26.699
Asymmetic Weight	IA50	56.819	47.475*	7.978	0.999	52.525**	4.694	0.697	44.247	1.134	8.098
Sparse	IA50	94.672	10.072**	7.852	0.994	89.928*	5.893	0.848	69.294	1.136	11.391
Stationary Input	IA50	48.617	56.872*	7.96	0.998	43.128**	4.768	0.694	41.442	1.113	6.561
Reduced Weight	IA12	100	0**	-	-	100*	1.882	0.79	71.785	1.415	24.187
Asymmetic Weight	IA12	55.709	50.969*	7.984	1	49.031**	4.669	0.692	45.307	1.152	8.649
Sparse	IA12	83.92	23.267**	7.882	0.996	76.733*	5.37	0.798	62.819	1.121	11.394
Stationary Input	IA12	49.481	57.518*	7.914	0.996	42.482**	4.532	0.671	40.884	1.129	7.42

* indicates significant increase in value due to variation ($t \geq 3.25$).

** indicates significant decrease in value due to variation ($t \leq -3.25$).

Note: Only the % of Core and % of Dynamic triads were subjected to significance tests

Table VIII – Parameter Triad Core Distributions

		CORE TRIAD TYPES												
CONDITION	INPUT	T1	T2	T3	T4	T5	T6	T7	T8	T9	T10	T11	T12	T13
Reduced Rate	RS	103889	118364	104777	0	13581	0	20	0	0	0	0	0	0
Reduced Window	RS	93715	106525	100163	0	12041	0	0	0	0	0	0	0	0
symmetric STDP	RS	93314	101782	95759	0	11443	0	0	0	0	0	0	0	0
Reduced Rate	RA	101427	121168	105411	0	13868	0	67	0	0	0	0	0	0
Reduced Window	RA	91013	107431	100871	0	12061	0	13	0	0	0	0	0	0
symmetric STDP	RA	93817	106177	98266	0	12074	0	17	0	0	0	0	0	0
Reduced Rate	IS	102512	112806	103384	0	12966	0	9	0	0	0	0	0	0
Reduced Window	IS	95457	104841	98717	0	11815	0	0	0	0	0	0	0	0
symmetric STDP	IS	93751	100094	96310	0	11416	0	0	0	0	0	0	0	0
Reduced Rate	IA50	106581	126337	110402	0	14586	0	186	0	0	0	0	0	0
Reduced Window	IA50	91813	113738	103089	0	12750	0	48	0	0	0	0	0	0
symmetric STDP	IA50	96926	106957	97002	0	12235	0	11	0	0	0	0	0	0
Reduced Rate	IA12	100363	125971	108693	0	14319	0	214	0	0	0	0	0	0
Reduced Window	IA12	86354	107842	100369	0	11970	0	85	0	0	0	0	0	0
symmetric STDP	IA12	92818	107251	97229	0	12152	0	46	0	0	0	0	0	0

		CORE TRIAD TYPES												
CONDITION	INPUT	T1	T2	T3	T4	T5	T6	T7	T8	T9	T10	T11	T12	T13
Reduced Weight	RS	57503	20827	42211	0	2640	0	0	0	0	0	0	0	0
Asymmetric Weight	RS	89770	94582	91358	0	10712	0	0	0	0	0	0	0	0
Sparse	RS	20083	19121	19068	0	1005	0	2	0	0	0	0	0	0
Stationary Input	RS	92414	101100	94998	29	10870	122	41	0	0	1	6	0	0
Reduced Weight	RA	26202	1218	10210	0	143	0	0	0	0	0	0	0	0
Asymmetric Weight	RA	79662	87360	87262	0	9641	0	0	0	0	0	0	0	0
Sparse	RA	19774	18272	18221	0	971	0	1	0	0	0	0	0	0
Stationary Input	RA	85638	92320	89206	65	9873	226	56	0	0	6	8	0	0
Reduced Weight	IS	34065	21674	38231	0	1824	0	0	0	0	0	0	0	0
Asymmetric Weight	IS	87354	89840	90688	0	10163	0	0	0	0	0	0	0	0
Sparse	IS	19416	24474	22521	0	1219	0	0	0	0	0	0	0	0
Stationary Input	IS	89971	98485	94840	13	10549	59	8	0	0	1	5	0	0
Reduced Weight	IA50	0	0	0	0	0	0	0	0	0	0	0	0	0
Asymmetric Weight	IA50	87654	86338	85757	0	9923	0	0	0	0	0	0	0	0
Sparse	IA50	13052	6095	6877	0	331	0	0	0	0	0	0	0	0
Stationary Input	IA50	82815	93292	90008	51	10070	142	24	2	1	1	9	0	0
Reduced Weight	IA12	0	0	0	0	0	0	0	0	0	0	0	0	0
Asymmetric Weight	IA12	85481	96695	90999	0	10677	0	9	0	0	0	0	0	0
Sparse	IA12	19437	16953	16692	0	881	0	3	0	0	0	0	0	0
Stationary Input	IA12	83211	98105	92423	50	10421	227	69	1	0	9	8	0	0

Table IX – Parameter Triad Dynamic Distributions

		DYNAMIC TRIAD TYPES					
CONDITION	INPUT	T1	T2	T3	T4	T5	T6
Reduced Rate	RS	9487.02 (1793.32)	19591.87 (3773.29)	12919.43 (1059.9)	155 (371.33)	2113.78 (324.59)	333.7 (465.82)
Reduced Window	RS	15950.52 (437.41)	26063.12 (1231.44)	14547.13 (561.58)	53.53 (106.7)	3009.88 (134.4)	136.77 (171.54)
symmetric STDP	RS	21781.97 (265.77)	42516.4 (1260.02)	24663.72 (694.78)	189.25 (84.26)	4946.13 (122.7)	358.17 (188.03)
Reduced Rate	RA	12875.28 (163.87)	29212.6 (550.42)	18167.03 (352.05)	293.67 (53.35)	3058.98 (63.61)	544.52 (142.43)
Reduced Window	RA	20226.38 (1147.51)	35474.82 (2272.15)	19085.03 (1169.01)	88.52 (640.36)	4052.55 (345.98)	233.77 (641.62)
symmetric STDP	RA	22018.65 (522.65)	46233.52 (994.92)	26555.27 (522.92)	191.3 (60.87)	5271.33 (106.9)	404.85 (124.06)
Reduced Rate	IS	8926.53 (281.11)	16529.3 (533.14)	10619.08 (302.48)	104.85 (29.72)	1851.13 (63.81)	308.9 (76.88)
Reduced Window	IS	14364.07 (356.73)	24474.98 (663.17)	14422.22 (341.48)	27.45 (35.8)	2941.27 (95.07)	109.05 (88.34)
symmetric STDP	IS	20385.28 (484.97)	36079.02 (1239.95)	20210.62 (735.96)	69.78 (67.97)	4257.8 (149.9)	178.17 (160.97)
Reduced Rate	IA50	12279.92 (236.18)	28765.7 (948.07)	17702.23 (574.02)	218.57 (83.55)	2991.73 (102.39)	457.07 (139.37)
Reduced Window	IA50	19351.72 (226.97)	35919.33 (717.5)	19688.9 (392.88)	51.37 (55.05)	3988.57 (86.9)	129.73 (104.2)
symmetric STDP	IA50	22737.33 (1173.82)	51156.33 (2237.75)	30512.67 (1151.29)	214.62 (844.58)	5759.13 (380.24)	491.27 (854.45)
Reduced Rate	IA12	14063.07 (443.02)	33122.35 (609.7)	20137.65 (371.67)	261.77 (35.61)	3494.48 (75.5)	606.75 (85.26)
Reduced Window	IA12	23933.37 (417.77)	44891.18 (1067.79)	24099.33 (560.16)	129.9 (50.26)	4861.18 (125.23)	308.63 (119.57)
symmetric STDP	IA12	24070.18 (307.97)	52988.72 (773.11)	30915.98 (390.81)	249.9 (78.24)	5955.97 (93.2)	619.58 (153.27)

		DYNAMIC TRIAD TYPES					
CONDITION	INPUT	T1	T2	T3	T4	T5	T6
Reduced Weight	RS	83811.15 (288.84)	168998.33 (1004.08)	90524.12 (526.23)	3567.22 (88.05)	18306.15 (114.22)	5048.75 (153.48)
Asymmetric Weight	RS	21290.15 (733.92)	41653.92 (1752.93)	25140.52 (797.96)	91.22 (334.67)	4798.42 (183.9)	269.35 (380.99)
Sparse	RS	18874.03 (439.61)	45821.29 (874.68)	24569.8 (502.55)	157.33 (87.5)	2405.08 (101.33)	211.23 (215.19)
Stationary Input	RS	6444.23 (425.28)	11929.8 (937.34)	7506.53 (435.48)	61.17 (68.47)	1408.12 (56.99)	152.58 (90.16)
Reduced Weight	RA	134792.77 (880.17)	274518.41 (2414.39)	144785.61 (840.73)	10585.35 (579.99)	27601.77 (288.98)	12131.2 (638.86)
Asymmetric Weight	RA	30515.97 (197.66)	57481.33 (526.23)	32537.7 (337.98)	127.23 (43.25)	6380.88 (51.76)	328.38 (99.09)
Sparse	RA	19758.62 (182.92)	49923.72 (523.24)	27345.68 (346.36)	168 (34.78)	2540.7 (61.88)	229 (94.05)
Stationary Input	RA	14174.05 (421.12)	26569.57 (848.28)	16203.85 (406.65)	59.68 (57.98)	3017.45 (51.1)	194.15 (77.74)
Reduced Weight	IS	81200.95 (255.51)	149477.77 (713.7)	86207.38 (437.98)	2465.88 (49.35)	15819.67 (86.15)	4046.43 (115.48)
Asymmetric Weight	IS	21690.62 (255.07)	36840.77 (515.7)	21543.3 (222.01)	51.27 (40.97)	4372.38 (54.4)	139.45 (75.74)
Sparse	IS	11054.68 (235.68)	20708.07 (550.99)	10632.43 (212.41)	34.05 (33.92)	1121.28 (44.11)	45.57 (65.15)
Stationary Input	IS	7058.87 (385.83)	10913.18 (867.07)	5778.02 (373.46)	24.6 (80.25)	1222.82 (54.16)	64.72 (123.76)
Reduced Weight	IA50	143441.56 (282.34)	286914.97 (1335.39)	142739.97 (716.39)	9439.57 (93.87)	24505.55 (135.47)	9378.05 (165.65)
Asymmetric Weight	IA50	26974.52 (295.11)	60238.85 (845.31)	37262.21 (526.37)	108.98 (52.8)	6676.75 (97.47)	292.27 (124.39)
Sparse	IA50	33434.52 (356.59)	79817.63 (941.69)	44348.68 (505.48)	222.73 (54.57)	4048.08 (105.43)	279.83 (129.58)
Stationary Input	IA50	20815.45 (361.24)	38401.2 (612.9)	22764.03 (291.75)	106.23 (29.41)	4373.17 (42.26)	204.62 (33.37)
Reduced Weight	IA12	158617.36 (379.34)	317333.28 (1182.73)	157367.44 (560.35)	20635.18 (65.72)	28823.12 (123.69)	20508.2 (128.09)
Asymmetric Weight	IA12	25621.62 (278.78)	56551.29 (959.97)	34010.52 (524.45)	168.67 (71.68)	6313.18 (115.74)	426.65 (152.24)
Sparse	IA12	21565.08 (275.02)	55966.88 (821.2)	30297.4 (388.22)	200.45 (76.67)	2836.27 (101.36)	290.67 (120.04)
Stationary Input	IA12	20438.15 (388.99)	38473.88 (841.64)	22180.93 (383.51)	99.72 (80.6)	4262.15 (58.05)	227.2 (104.93)

Table IX Continued

		DYNAMIC TRIAD TYPES						
CONDITION	INPUT	T7	T8	T9	T10	T11	T12	T13
Reduced Rate	RS	176.78 (165.09)	8.02 (19.27)	0.05 (8.4)	4.7 (25.11)	17.3 (27.8)	0 (2.39)	0 (0.22)
Reduced Window	RS	68.67 (36.86)	2.67 (5.49)	0.05 (0.72)	0.9 (5.36)	6.87 (10.3)	0 (0.22)	0
symmetric STDP	RS	234.05 (47.35)	10.77 (5.81)	0.38 (0.89)	5.03 (7.68)	21.18 (12.54)	0.05 (0.28)	0
Reduced Rate	RA	403.9 (11.62)	12.53 (3.21)	0.73 (0.25)	13.57 (2.62)	30.4 (7.89)	0.15 (0.18)	0
Reduced Window	RA	207.92 (128.63)	5.03 (35.63)	0.1 (23.79)	3.42 (60.42)	13.48 (33.22)	0.03 (6.31)	0 (0.18)
symmetric STDP	RA	435.73 (35.41)	12.43 (3.73)	0.38 (0.47)	9.93 (3.9)	23.63 (7.72)	0.05 (0.29)	0
Reduced Rate	IS	73.3 (7.5)	4.87 (2.59)	0.07 (0)	2.78 (0.7)	16.95 (4.43)	0.03 (0.13)	0
Reduced Window	IS	42.05 (22.35)	1.92 (2.34)	0 (0.18)	0.47 (3.22)	6.12 (5.36)	0.02 (0.18)	0
symmetric STDP	IS	78.97 (43.74)	4.48 (4.68)	0.07 (0.7)	1.12 (5.38)	9.6 (9.92)	0 (0.39)	0
Reduced Rate	IA50	468.05 (33.52)	11.88 (5.65)	0.47 (0.8)	14.32 (4.75)	26.05 (9.27)	0.05 (0.22)	0
Reduced Window	IA50	337.68 (12.8)	3.38 (3.79)	0.03 (0.25)	3.53 (1.03)	7.62 (6.17)	0.03 (0)	0
symmetric STDP	IA50	528.2 (129.17)	12.12 (45.59)	0.42 (62.3)	12.08 (80)	29.72 (44.93)	0.1 (12.76)	0 (0.83)
Reduced Rate	IA12	589.83 (9.87)	12.88 (2.6)	0.77 (0.22)	19.07 (1.24)	33.93 (4.92)	0.08 (0.13)	0
Reduced Window	IA12	503.75 (33.37)	6.65 (3.85)	0.18 (0.46)	8.07 (3.31)	17.9 (7.12)	0.05 (0.22)	0
symmetric STDP	IA12	665.47 (28.55)	13.97 (5.72)	0.92 (0.65)	19.33 (5.49)	35.92 (9.41)	0.13 (0.3)	0

		DYNAMIC TRIAD TYPES						
CONDITION	INPUT	T7	T8	T9	T10	T11	T12	T13
Reduced Weight	RS	2120.92 (26.99)	164.37 (5.81)	49.93 (0.74)	193.45 (3.15)	265.1 (9.71)	4.73 (0.22)	0
Asymmetric Weight	RS	168.15 (80.46)	5.55 (21.15)	0.25 (9.25)	3.98 (21.15)	16.22 (24.28)	0.02 (2)	0
Sparse	RS	499.52 (42.61)	3.43 (5.76)	0.27 (1.23)	6.55 (7)	5.33 (12.72)	0 (0.47)	0
Stationary Input	RS	18.97 (24.7)	2.02 (2.52)	0.53 (0.64)	2.25 (3.23)	8.23 (2.75)	0	0
Reduced Weight	RA	6621.9 (167.29)	458.28 (34.48)	239.35 (29.5)	885.23 (49.96)	613.43 (36.03)	38.8 (6.49)	0.45 (0.62)
Asymmetric Weight	RA	351.08 (10.07)	7.08 (2.84)	0.17 (0.22)	6.83 (1.09)	19.28 (4.91)	0.08 (0)	0
Sparse	RA	560.7 (7.87)	3.75 (2.35)	0.28 (0.51)	6.85 (0.97)	5.75 (7.05)	0	0
Stationary Input	RA	46.97 (23.8)	2.58 (2.09)	0.2 (0.48)	2.8 (3.25)	12.65 (3.19)	0	0
Reduced Weight	IS	1390.87 (21.61)	121.18 (3.48)	27.88 (0.35)	145.67 (2.65)	219.82 (7.91)	5.85 (0.18)	0.05 (0)
Asymmetric Weight	IS	49.88 (14.26)	2.85 (1.77)	0.05 (0.5)	0.88 (2.13)	7.58 (5.01)	0.02 (0)	0
Sparse	IS	77.48 (19.06)	0.92 (1.51)	0.02 (0.43)	0.77 (2.63)	0.63 (5.48)	0	0
Stationary Input	IS	10.98 (23.64)	0.98 (3.12)	0.23 (0.91)	1.43 (4.16)	4.83 (3.28)	0 (0.13)	0
Reduced Weight	IA50	8089.65 (42.93)	404.37 (5.67)	156.88 (0.94)	810.13 (5.81)	409.35 (9.6)	27.7 (0.4)	0.03 (0)
Asymmetric Weight	IA50	432.93 (17.63)	5.85 (3.56)	0.17 (0.44)	5.8 (2.55)	15.68 (7.89)	0.05 (0.13)	0
Sparse	IA50	879.6 (27.33)	5.62 (4.33)	0.5 (0.38)	9 (2.76)	6.85 (8.66)	0.08 (0.18)	0
Stationary Input	IA50	179.4 (13.21)	4.5 (1.36)	1.05 (0.13)	5.35 (1.28)	11.7 (1.07)	0.52 (0)	0
Reduced Weight	IA12	9739.23 (35.56)	944.87 (4.16)	687.32 (0.42)	1907.55 (3.86)	951.82 (7.61)	124.12 (0.28)	0.87 (0)
Asymmetric Weight	IA12	581.82 (20.07)	10.1 (4)	0.42 (0.22)	11.37 (3.08)	24.85 (8.08)	0.13 (0)	0
Sparse	IA12	627.52 (30.98)	5.03 (3.76)	0.5 (1.61)	8.75 (4.78)	5.98 (7.41)	0.02 (0.81)	0
Stationary Input	IA12	208.5 (28.74)	6.12 (2.64)	0.17 (0.75)	4.37 (4.95)	14.35 (3.75)	0.03 (0.28)	0

Values in parentheses are s.d.'s across time

References

Acer UG, Drineas P, Abouzeid AA (2011) Connectivity in time-graphs. Pervasive and Mobile Computing 7:160-171.

Brunel N (2000) Dynamics of sparsely connected networks of excitatory and inhibitory spiking neurons. J Comput Neurosci 8:183-208.

Buchel C, Coull JT, Friston KJ (1999) The predictive value of changes in effective connectivity for human learning. Science 283:1538-1541.

Bullmore E, Sporns O (2009) Complex brain networks: graph theoretical analysis of structural and functional systems. Nat Rev Neurosci 10:186-198.

Diesmann M, Gewaltig MO, Aertsen A (1999) Stable propagation of synchronous spiking in cortical neural networks. Nature 402:529-533.

Dijkstra E (1959) A note on two problem in connexion with graphs. Numerische Mathematik 1:269-271.

Fagiolo G (2007) Clustering in complex directed networks. Physical Review E 76:8.

Fino E, Venance L (2010) Spike-timimg dependent plasticity in the striatum. Frontiers in Synaptic Neurosci 2:1-10.

Fino E, Paille V, Cui YH, Morera-Herreras T, Deniau JM, Venance L (2010) Distinct coincidence detectors govern the corticostriatal spike timing-dependent plasticity. Journal of Physiology-London 588:3045-3062.

Grindrod P, Higham DJ (2010) Evolving graphs: dynamical models, inverse problems and propagation. Proc R Soc A-Math Phys Eng Sci 466:753-770.

Haas JS, Nowotny T, Abarbanel HDI (2006) Spike-timing-dependent plasticity of inhibitory synapses in the entorhinal cortex. J Neurophysiol 96:3305-3313.

Izhikevich EM (2004) Which model to use for cortical spiking neurons? Ieee Transactions on Neural Networks 15:1063-1070.

Jacob V, Brasier DJ, Erchova I, Feldman D, Shulz DE (2007) Spike timing-dependent synaptic depression in the in vivo barrel cortex of the rat. Journal of Neuroscience 27:1271-1284.

Kim H, Tang J, Anderson R, Mascolo C (2012) Centrality prediction in dynamic human contact networks. Comput Netw 56:983-996.

Kozloski J, Cecchi GA (2010) A theory of loop formation and elimination by spike timing-dependent plasticity. Front Neural Circuits 4:11.

Kunkel S, Diesmann M, Morrison A (2011) Limits to the development of feed-forward structures in large recurrent neuronal networks. Front Comput Neurosci 4:15.

Li CG (2008) Functions of neuronal network motifs. Physical Review E 78.

Markram H, Lubke J, Frotscher M, Sakmann B (1997) Regulation of synaptic efficacy by coincidence of postsynaptic APs and EPSPs. Science 275:213-215.

Masuda N, Kori H (2007) Formation of feedforward networks and frequency synchrony by spike-timing-dependent plasticity. J Comput Neurosci 22:327-345.

McIntosh AR, Rajah MN, Lobaugh NJ (2003) Functional connectivity of the medial temporal lobe relates to learning and awareness. Journal of Neuroscience 23:6520-6528.

Milo R, Shen-Orr S, Itzkovitz S, Kashtan N, Chklovskii D, Alon U (2002) Network motifs: Simple building blocks of complex networks. Science 298:824-827.

Milo R, Kashtan N, Itzkovitz S, Newman M, Alon U (2003) Uniform generation of random graphs with arbitrary degree sequences. cond-mat/0312028.

Milo R, Itzkovitz S, Kashtan N, Levitt R, Shen-Orr S, Ayzenshtat I, Sheffer M, Alon U (2004) Superfamilies of evolved and designed networks. Science 303:1538-1542.

Onnela JP, Saramaki J, Kertesz J, Kaski K (2005) Intensity and coherence of motifs in weighted complex networks. Physical Review E 71:4.

Reijneveld JC, Ponten SC, Berendse HW, Stam CJ (2007) The application of graph theoretical analysis to complex networks in the brain. Clin Neurophysiol 118:2317-2331.

Ren QS, Kolwankar KM, Samal A, Jost J (2009) STDP-driven networks and the C. elegans neuronal network. Physica A 389:3900-3914.

Reyes AD (2003) Synchrony-dependent propagation of firing rate in iteratively constructed networks in vitro. Nature Neuroscience 6:593-599.

Robinson PA, Henderson JA, Matar E, Riley P, Gray RT (2009) Dynamical Reconnection and Stability Constraints on Cortical Network Architecture. Phys Rev Lett 103:4.

Rubinov M, Sporns O (2010) Complex network measures of brain connectivity: Uses and interpretations. Neuroimage 52:1059-1069.

Scherrer A, Borgnat P, Fleury E, Guillaume JL, Robardet C (2008) Description and simulation of dynamic mobility networks. Comput Netw 52:2842-2858.

Shin CW, Kim S (2006) Self-organized criticality and scale-free properties in emergent functional neural networks. Physical Review E 74:4.

Song S, Miller KD, Abbott LF (2000) Competitive Hebbian learning through spike-timing-dependent synaptic plasticity. Nature Neuroscience 3:919-926.

Song S, Sjostrom PJ, Reigl M, Nelson S, Chklovskii DB (2005) Highly nonrandom features of synaptic connectivity in local cortical circuits. PLoS Biol 3:507-519.

Sporns O, Kotter R (2004) Motifs in brain networks. PLoS Biol 2:1910-1918.

Starnini M, Baronchelli A, Barrat A, Pastor-Satorras R (2012) Random walks on temporal networks. Physical Review E 85.

Suzuki T, Ikeguchi T (2005)Transition from random to small-world neural networks by STDP learning rule. 2005 RISP International Workshop on Nonlinear Circuit and Signal Processing: 17-20.

Takahashi YK, Kori H, Masuda N (2009) Self-organization of feed-forward structure and entrainment in excitatory neural networks with spike-timing-dependent plasticity. Physical Review E 79:10.

Watts DJ, Strogatz SH (1998) Collective dynamics of 'small-world' networks. Nature 393:440-442.

Yu LP, Stein BE, Rowland BA (2009) Adult Plasticity in Multisensory Neurons: Short-Term Experience-Dependent Changes in the Superior Colliculus. Journal of Neuroscience 29:15910-15922.

Appendix A - Rate Correlated Learning

In addition to the STDP learning implementation, an additional simulation was performed using a different learning rule that did not depend on the specific timing of pre-synaptic and post-synaptic neurons. Rather, a learning implementation was applied which depended on correlations in firing rate activity between the pre- and post-synaptic neurons. Measures of topological dynamics were collected across an analysis interval of the same duration as in the STDP simulations for comparison.

Learning Rule Implementation and Simulation

The basic principle of the rate learning algorithm was to modify synapses based on comparisons between the firing rates of the pre-synaptic and post-synaptic neurons. When the firing rates of both neurons were increasing or decreasing, the synapse connecting the two neurons was potentiated according to the following set of equations:

Eq. A1
$$\Delta w_t = \Delta w_{t-1} + A_+ \left(r_{pre} - \bar{r}_{pre}\right)\left(r_{post} - \bar{r}_{post}\right)$$

Eq. A2
$$A_+ = \begin{cases} \eta \Big/ \max\left[\left(r_{pre} - \bar{r}_{pre}\right)\left(r_{post} - \bar{r}_{post}\right)\right] & \text{if } \max\left[\left(r_{pre} - \bar{r}_{pre}\right)\left(r_{post} - \bar{r}_{post}\right)\right] > \eta \\ 1 & \text{otherwise} \end{cases}$$

And when the firing rate of one neuron was increasing while the other was decreasing, the synapse was depressed:

Eq. A3
$$\Delta w_t = \Delta w_{t-1} + A_- \left(r_{pre} - \bar{r}_{pre}\right)\left(r_{post} - \bar{r}_{post}\right)$$

Eq. A4
$$A_- = \begin{cases} -\eta \Big/ \min\left[\left(r_{pre} - \bar{r}_{pre}\right)\left(r_{post} - \bar{r}_{post}\right)\right] & \text{if } \min\left[\left(r_{pre} - \bar{r}_{pre}\right)\left(r_{post} - \bar{r}_{post}\right)\right] < -\eta \\ 1 & \text{otherwise} \end{cases}$$

In *Eq. A1 - A4*, $\Delta\omega_t$ is the additive (+/-) change in synaptic weight, $\Delta\omega_{t-1}$ is the value of $\Delta\omega$ from the preceding timestep. r_{pre} and r_{post} are the firing rates of the pre- and post-

synaptic neurons, respectively, averaged over the last 1000 timepoints (the last second). Specifically, r_{pre} and r_{post} are the sum of the number of firings for each neuron from timepoint t - 999 to t where t is the current timepoint. $\bar{r}_{pre}$ and $\bar{r}_{post}$ are the mean firing rates of the pre- and post-synaptic neurons, respectively. $\bar{r}_{pre}$ and $\bar{r}_{post}$ are the sum of the number of firings from each neuron from timepoint t - 4999 to t divided by five. A_+ and A_- determine the maximum or minimum weight change for a given synaptic event (learning rate). η is a scaling factor that bounds the maximum and minimum attainable weight from any synaptic event. η is set to 0.044 (0.055% of the maximum attainable weight) to maintain consistency with the STDP simulations. Max and min are the maximum and minimum functions evaluating $\left(r_{pre} - \bar{r}_{pre}\right)\left(r_{post} - \bar{r}_{post}\right)$ over all synapses connecting the pre-synaptic neuron to all of its post-synaptic neurons. Note that when the firing rate of either neuron was constant, the synapse remained unmodified.

Eq. A1 - A4 are evaluated every time a pre-synaptic neuron fires (i.e. every time there is a change in the pre-synaptic firing rate). As with the STDP implementation, the synapse was updated only once every 1000 timesteps (once per second) by adding the current value of $\Delta\omega$ at that timepoint to the current weight. Synaptic weights were bounded so that when the sum of the synaptic weight and $\Delta\omega$ was > 8 mV or < 0 mV, the weight was set to 8 mV or 0 mV, respectively.

The simulation was initialized with five seconds of activity (5000 timepoints) during which external input was provided and neurons fired, but $\Delta\omega$ remained zero and synapses weren't modified. This initialization was necessary to determine the firing rates and mean firing rates so that $\Delta\omega$ could be evaluated.

All other aspects of the simulation were the same as the standard STDP simulations. The initial network was selected from one of the 10 original networks used the standard simulations and external input was irregular, asynchronous input at 12 Hz (IA12). The simulation was run for the same duration (7.2 million timepoints) with the same analysis interval. The same measures were collected and evaluated as in the standard simulations.

Results and Conclusions

Table AI presents the values obtained from all measures in the simulation as well as the averages of the same measures from the 10 STDP simulations where the same external input was used (IA12). Remarkably, no functional motifs were detected in the simulation using the modified learning rule. The average firing rate and average synaptic weight from the correlated rate learning simulation were much higher than in the STDP simulations. These results imply that pre- and post-synaptic firing rates were frequently or highly correlated. It is possible that $\Delta\omega$ reached maximal values quickly, further increasing correlations until synaptic modification no longer occurred. Indeed, all of the remaining excitatory-to-excitatory synaptic weights reached 8 mV. As mentioned previously, the difference between the maximum attainable synaptic weight and the learning rate can have significant consequences on network (and triad) behavior. These parameters were selected to maintain consistency with the STDP simulations. It is possible that variations in these parameters could result in more interesting behavior for the rate correlation learning implementation. At any rate, the triad type distribution from the simulation was qualitatively different than the STDP distributions as displayed in Figure A1, further underscoring differences in network topology between the two different learning regimes. Taken together,

these results suggest that STDP may be unique in developing and maintaining the stable yet dynamic sorts of topologies which were observed in the original simulations.

Table AI – Rate Learning Results

		RATE LEARN	STDP
1	total synapses per min	15906	9249.361667
2	ave wt per min	7.966	4.5669
3	ave path per min	0.2395	2.617848186
4	ave clust coeff per min	0.7987	0.44244716
5	ave total degree per min	79.53	47.3457
6	# remaining triads (observed at least once)	992395	569135.4
7	% of remaining triads observed	99.268	56.7712
8	% of core triads	100	50.0836
9	avera core intensity	8	7.9816
10	ave core coherence	1	0.9997
11	% of functional triads	0	49.9164
12	ave funct intensity	NaN	4.6958
13	ave funct coherence	NaN	0.6946
14	% time as a triad	NaN	44.5536
15	ave repertoire size	NaN	1.1529
16	ave number of changes	NaN	8.3517
17	ave net change in triad number	0	2001.3236
18	ave gained	0	18237.4423
19	ave lost	0	18242.356
20	ave firing rate	112.5635	12.593
21	CV num synapses	0	0.002320085
22	CV ave wts	0	0.001532275
23	CV ave path len	0	2.079907221
24	CV ave clust coeff	0	0.003792791
25	CV ave neuro degree	0	0.002616169
26	Gained to net ratio	NaN	9.227899598
27	lost to net ratio	NaN	9.229889106

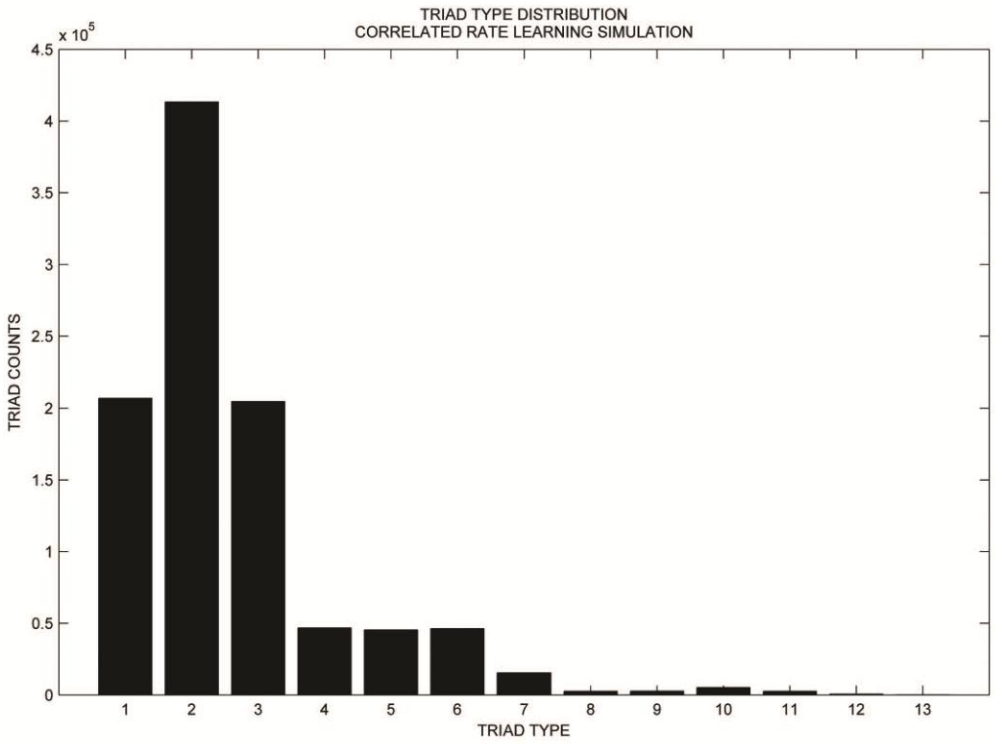

Figure AI – Type Distribution Rate Learning

Appendix B - Matlab Code for STDP Simulations

The following code is a stand-alone variation of the primary code used in the STDP simulations.

```
%stdp net-----------------------------------------------------------------
%This is the main program for running stdp net simulations as used in
%mauscript.
%It creates an initial weight matrix and applies input (regular synchronous, 50Hz)
%for one hour while modifying weights according to STDP learning rule.
%Displays a rastergram, weight distribution, and input matrix during each second.
%Main output is a multidim matrix 'W', which contains the weight matrix at each
minute of simulation.
%
%Code for the STDP implementation was inspired by Izhikevich, 2005
%and can be found at:
%http://senselab.med.yale.edu
%titled: spnet.m
%
%Written by David B. Stone, 2010 - 2012
%-------------------------------------------------------------------------------


%-----Parameters-----------------------------------------------------------------
N = 500;   %number of neurons
E = round(.8*N);    %# of excitatory
In = round(.2*N);   % In = N - E;       # of inhibitory
num_conn = round(.1*N); %# of synapses
a=[0.02*ones(E,1); .1*ones(In,1)];  %} a,b,c,d are neuron dynamical params
b = .2;                             %
c = -65;                            %
d=[8*ones(E,1); 2*ones(In,1)];      %
max_w = 8; %maximum weight per synapse
v = c;  %voltage (initially a scalar, becomes an N-by-1 vector)
u = 0.2.*v; %relaxation variable
ftimes = zeros(N,1002); %a neuro-by-timepoint matrix of current stdp value(voltage)
dw = zeros(N);      %differential weight matrix (updated ea ms according to stdp)
%-------------------------------------------------------------------------------

%----Create an initial network---------------------------------------------
A = zeros(N); %Adjacency (binary) matrix
for i = 1:N
    p = randperm(N);    %shuffle neurons
    q = round((5*randn)+num_conn); %pick #ofconnects from normdistrib(mean
                                                        %num_conn,var 25)
    h = p(1:q); %pick post syn neuros
    A(i,h)=1;
end;
%make the diagonal zeros (no self-connecting neurons)
diagonal = diag(A);
diagonal = diag(diagonal);
A = A-diagonal;

w = zeros(N);       %weight matrix
ind = find(A);
for i = 1:length(ind)
    w(ind(i)) = max_w*rand;  % uniform distr of weights (range from 0 to max_w)
end;
```

```
w(E+1:N,:) = -1 .* w(E+1:N,:); %make the inhib neuros negative
%--------------------------------------------------------------------------

%index of pre- and post-synaptic neurons for each neuron
pre = cell(N,1);
post = cell(N,1);
for i = 1:N
    pre{i} = find(w(:,i));
    post{i} = find(w(i,:));
end;

%multidim matrix of weights each minute
W = zeros(N,N,61);
W(:,:,1) = w;       %Initial weight matrix

%--------Simulation (one hour)-----------------------------------------
for mins = 2:61     %minutes. min(1) is initial weight matrix

    for s = 1:60    %seconds

        %Input (Regular Synchronous)-------------------------------------
        P = zeros(N,1000);  %input matrix (neurons-by-time)
        pt = linspace(1,981,50);    %50 = every 20 spaces (50Hz)
        for i = 1:50 %length of pt
            z= randperm(500);
            e = uint16(100+randn);
            z = z(1:e); %pick ~100 random neurons
            P(z,pt(i)) = 16; %16 mV input
        end;
        %----------------------------------------------------------------

        for t = 1:1000  %millisecs

            I = .5*randn(N,1)+1.3;   %weak internal noise term
            I = I + P(:,t);          %external input
            F = find(v>=30); %index of neurons that fired at t-1 (at last ms)
            v(F)=c;
            u(F)=u(F)+d(F);
            ftimes(F,t+1) = .044; %= learning rate

            for i = 1:length(F) %for ea fired neuro
                I(post{F(i)}) = I(post{F(i)}) + w(F(i),post{F(i)})'; %synaptic
                                                                      %input
                %pre->post stdp
                dw(pre{F(i)},F(i)) = dw(pre{F(i)},F(i)) + ftimes(pre{F(i)},t);

                %post->pre stdp
                dw(F(i),post{F(i)})=dw(F(i),post{F(i)})1.05*ftimes(post{F(i)},t)';

            end;

            ftimes(:,t+2) = 0.95*ftimes(:,t+1); %reduce potentiation
                                                %[(A+)e^(-t/20)=stdp
rule]

            %Runge Kutta ------------------------
            h = .5;

            v1 = v;
            k1 = h*((.04*v1+5).*v1+140-u+I);
            v2 = (v +.5.*k1);
            k2 = h*((.04*v2+5).*v2+140-u+I);
```

```
            v3 = (v+.5.*k2);
            k3 = h*((.04*v3+5).*v3+140-u+I);
            v4 = (v + k3);
            k4 = h*((.04*v4+5).*v4+140-u+I);
            v = v + (1/6).*(k1 + 2*k2 + 2*k3 + k4); %update voltage (4th order

            v1 = v;
            k1 = h*((.04*v1+5).*v1+140-u+I);
            v2 = (v +.5.*k1);
            k2 = h*((.04*v2+5).*v2+140-u+I);
            v3 = (v+.5.*k2);
            k3 = h*((.04*v3+5).*v3+140-u+I);
            v4 = (v + k3);
            k4 = h*((.04*v4+5).*v4+140-u+I);
            v = v + (1/6).*(k1 + 2*k2 + 2*k3 + k4); %do it again

            if max(v) > 30
                v_ind = find(v>=30);
                v(v_ind) = 30;  %bound max voltage to 30 mV
            end;

            u1 = u;
            ku1 = a.*(b.*v-u1);
            u2 = u + .5.*ku1;
            ku2 = a.*(b.*v-u2);
            u3 = u + .5.*ku2;
            ku3 = a.*(b.*v-u3);
            u4 = u + ku3;
            ku4 = a.*(b.*v-u4);
            u = u + (1/6).*(ku1 + 2*ku2 + 2*ku3 + ku4); %update relaxation term
            %-----------------------------------------------

        end;

        %----- Plot ----------------------------------%
        [x,y] = find(ftimes==.044);
        ind = (w ~= 0);
        wt = w(ind);
        subplot(3,1,1);
        plot(y,x,'k.'); %rastergram
        title(s);
        axis([0 1000 0 N]); drawnow;
        subplot(3,1,2);
        hist(wt,100);   %weight distribution
        title(mins-1);
        axis([0 8 0 16500]);drawnow;
        subplot(3,1,3);
        image(P);drawnow    %external input
        %-------------------------------------------------%

        ftimes(:,1:2) = ftimes(:,1001:1002);    %wrap around
        w(1:E,1:E) = max(0,min(max_w,w(1:E,1:E)+dw(1:E,1:E)));  %update weights
        dw = .9*dw; %reduction term for stability

    end; %seconds

    W(:,:,mins) = w;    %weight matrix at each minute

end; %minutes
```